

# Non-destructive Techniques for Thermal Energy Storage Technologies

Joey Aarts<sup>1,2</sup> · Natalia Mazur<sup>5</sup> · Ruben D'Rose<sup>3</sup> · Stan de Jong<sup>1,2</sup> · Anders Kaestner<sup>4</sup> · Hartmut Fischer<sup>5</sup>

Received: 27 May 2025 / Accepted: 1 October 2025 © The Author(s) 2025

### **Abstract**

The understanding of processes in heat storage materials and reactors can be greatly improved by the use of non-destructive methods that allows the view inside the objects. The advantage of non-destructive methods is that the sample of interest remains intact, experimental changes can be monitored in-situ, and the experiments are less labor intensive. Alongside others, three of the most utilized non-destructive techniques for heat storage systems are discussed: NMR, X-ray imaging, and neutron imaging. The working mechanism and (dis)advantages of these techniques are discussed alongside various applications and examples. This work aims to provide a handle to researchers working in the field of thermal energy storage on how to investigate heat storage materials and reactors in a non-destructive manner.

**Keywords** Heat storage · Non-destructive · Neutrons · NMR · X-ray · Energy

### 1 Introduction

To tackle the current climate crisis, the European member states have agreed in the European Green Deal to reduce the greenhouse gases by 55% (compared to pre-industrial levels) by 2030 and to become fully climate neutral by 2050 [1]. Since space heating, cooling and hot tap water production are still major contributors to the total greenhouse gas emissions, sustainable heating alternatives must be implemented [2].

Currently many renewable energy sources are employed such as solar and wind energy. However, these energy sources provide an intermittent supply of energy and thus a mismatch between peak energy production and consumption exists [3]. To effectively utilize the available renewable energy sources or to revalorize waste heat streams, efficient energy storage is required.

Thermal energy storage can be divided according to three different working principles. First there is sensible heat storage (SHS) which relies on the heat capacity of the chosen heat storage material. Energy is stored by increasing the temperature of the heat storage material. A well-known example of sensible heat storage is the hot water tank [4].

Second, heat can be stored in the solid—liquid phase transition of materials. This is called latent heat storage (LHS), and the used heat storage materials are referred to as phase change materials (PCMs). Latent heat storage is associated with higher energy storage densities compared to sensible heat storage and well-known examples are ice, paraffins or salt hydrates [5].

- Eindhoven Institute of Renewable Energy Systems, Eindhoven University of Technology, PO Box 513, Eindhoven 5600 MB, the Netherlands
- Department of Applied Physics, Transport in Permeable Media Group, Eindhoven University of Technology, PO Box 513, Eindhoven 5600 MB, the Netherlands
- Department of Mechanical Engineering, Eindhoven University of Technology, Eindhoven University of Technology, PO Box 513, Eindhoven 5600 MB, the Netherlands
- Laboratory for Neutron Scattering and Imaging, Paul Scherrer Institute, Villigen, Switzerland
- <sup>5</sup> TNO Materials Solution, High Tech Campus 25, Eindhoven, Netherlands

☑ Joey Aarts j.aarts@tue.nl

> Natalia Mazur natalia.mazur@tno.nl

Ruben D'Rose r.d.d.rose@tue.nl

Stan de Jong s.j.d.jong@tue.nl

Anders Kaestner anders.kaestner@psi.ch

Hartmut Fischer hartmut.fischer@tno.nl

Published online: 10 October 2025



Third, there is thermochemical energy storage (TCHS) which relies on the interaction of a thermochemical material and a gas. This method of heat storage has the highest energy density, and some examples of materials often used are salt hydrates, metal hydroxides, metal carbonates, zeolites, metal organic frameworks, oxidation/reduction of iron, metal oxides, and silica gel [6].

In an application, the active heat storage material is often placed in a heat storage vessel as pure compound or as composite material [7–9]. Depending on the chosen working principle (sensible, latent, or thermochemical) the internal structure of the heat storage vessel can vary from pure heat storage material to stacked or packed bed configurations including or excluding additional structural modifications [8, 10–14].

Multiple modelling approaches exist to determine the performance of heat storage materials and vessels using indirect observation such as inlet/outlet and internal/external temperatures [4, 15], flow rates and pressure drop [12], or assumptions and available literature data [16–18]. However, such models lack information about the structure and morphology of the material, as well as information on the packing geometry of the heat storage vessel, treating it as a black box with assumptions which can result in deviations from reality.

Methods for characterizing thermal energy storage materials and systems can be classified into two categories. The first category comprises destructive techniques and often involves opening and dismantling the heat storage vessel or physical fracturing of material to examine the inside using optical techniques such as scanning electron and optical microscopy. This is labor intensive and destroys the sample of interest, possibly introducing artefacts in the process. The second category comprises non-destructive techniques that enable researchers to investigate the heat storage vessel without its disassembly.

To aid in the input for theoretical models, a detailed understanding of processes and changes during (dis)charge processes is required. In this work the various available non-destructive methods are described and will be discussed using examples. Coverage in literature is however limited. Many reviews of non-destructive techniques exist in the literature; however, they typically focus on visualizing and analyzing defects and various composite materials [19–22]. The primary techniques described in this work are nuclear magnetic resonance imaging, X-ray imaging and neutron imaging, as those are the three techniques that have been applied in heat storage research on number of occasions [23–25]. In the end, the methods will be compared and evaluated based on the information each technique provides, and they can serve as a starting point for other research into heat storage systems in which researchers want to investigate their material and heat storage vessels in a non-destructive way.

## 2 The Need for Non-destructive Techniques

The following section will illustrate the need for non-destructive techniques for thermal energy storage solutions. Often observations made on small scale or individual particles cannot be directly translated towards a full system and inside the heat storage vessel, often called a reactor, many structural changes during charging and discharging occur. These changes can impact on the overall system performance and should therefore be understood. For example, in sensible heat storage using a hot water tank, mixing of water or thermal stratification can occur resulting in separation of the liquid into layers of different temperatures. Figure 1 shows how thermal stratification in a hot water tank results in segregation of water into a bottom volume with colder water (blue) and a volume with warmer water (green) [15].

In LHS, phase segregation due to natural convection and density differences between solid and liquid phase often occur [26]. This results in a similar situation as described for stratification in a hot water tank with the difference that now the molten and solid phases will separate, just like melting ice floats on the surface of the already molten water.

In the case of TCHS, some changes occurring during (dis)charging can be a volumetric increase and decrease of salt hydrates, crack and dust formation, and agglomeration (Fig. 2) [27, 28]. All structural changes will have an impact on the performance of the heat storage unit and therefore understanding how these changes evolve over time is key for performance optimization. Figure 2A shows how particles of  $K_2CO_3 \cdot 1.5H_2O$  pressed to different porosities, by changing the compressive pressure during uniaxial pressing, evolve during cyclic (dis)charging before they eventually fracture. This fracturing occurs due to the internal morphological reorganization during cyclic (dis)charging. In Fig. 2B it is visible how grains of the same material increase their size during 12 (dis)charging cycles, causing the effects observed in Fig. 2A.

Apart from the observations highlighted in this section, other challenges associated with heat storage materials exist. For example, in latent heat storage phase change materials can suffer from incongruent melting, volume changes, or supercooling. Thermochemical materials can, in addition to the volumetric changes, suffer from poor reversibility and multiple hydration states. The use of non-destructive techniques allows researchers to observe those changes and effects as they happen. Additionally, the effect of reaction conditions or mechanical loads imposed by material confinement can be observed. Gaining such insight is invaluable for



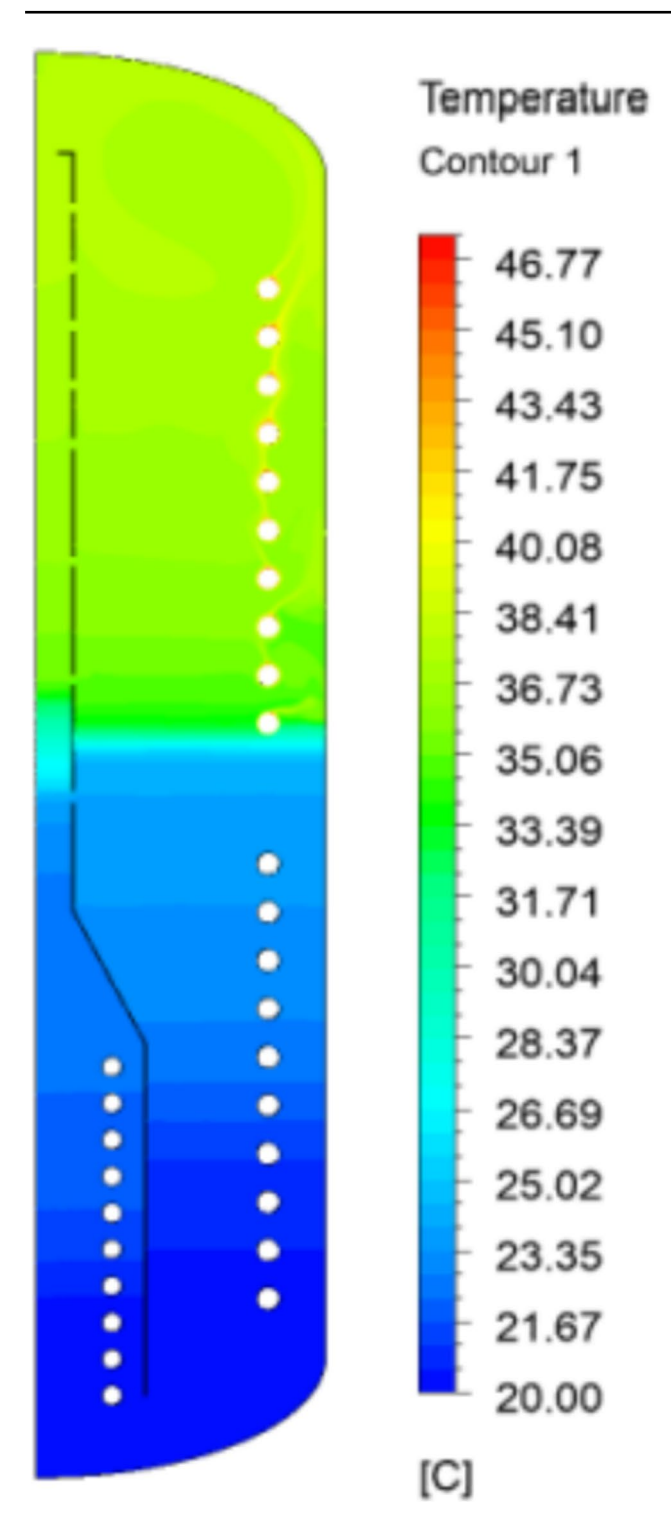


Fig. 1 Thermal stratification of a hot water tank showing the separation of hot and cold water throughout the tank. The white circles represent the 3 coiled heat exchangers present in the tank. Temperature profiles are generated via numerical modelling. Adapted from "Investigating Thermal Stratification in a Hot Water Storage Tank during Charging Mode," by K. Kumar, and S. Singh, 2022, Journal of Physics: Conference Series, 2178(1) (https://doi.org/10.1088/1742-6596/2178/1/012001). CC BY [17]

the design of better reactors and optimizing the operating conditions.

### 2.1 Optical Imaging

Various optical imaging techniques, often coupled with computer image processing, are commonly utilized to monitor the effect of (dis)charge cycles. Since they provide a field of view for a limited material volume from a fixed angle, it imposes limitations on the researchers. Such work often studies individual particles over the course of several cycles with either optical microscope [28] or scanning electron microscope [27]. Those investigations give information about particle swelling and crack formation that can be further used to develop and validate more fundamental processes occurring in heat storage materials material.

In LHS, this methodology is often employed to monitor the reaction progress in custom made see-through reactors. In many cases, PCMs turn from white, opaque to clear when they change phase from solid to liquid. Figure 3 shows how optical imaging can be utilized to monitor the melting behavior of PCM inside a container. Initially, the complete PCM volume is white and for the system with 1 or 3 fins the fins are clearly visible protruding from the wall into the PCM. As the temperature of the right wall (and fins) increases, a clear melting front of molten PCM (clear/black) can be seen to progress through the PCM from the hot (right) to the cold (left) side.

Visible changes are easily tracked with a standard camera and can be related to several properties. Most commonly values for conversion speed [29–31], temperature gradient within the material [29] and heat transfer rate [29] are extracted from the visual changes. It is however important to note that the extracted properties are only valid for coordinates in the imaging plane (2D). Information perpendicular to the imaging plane cannot be derived.

Additionally, the uniformity of the reaction, the heat transfer mechanism and the effect of other forces or phenomena, such as effect of buoyancy or phase segregation, might be noticeable, depending on the material and experimental conditions. For example, a non-uniform melting front might indicate non-uniform temperature distribution due to inhomogeneities in the studied material or presence of natural convection which promotes movement of hot, low-density liquid to the top of the tank.

In TCHS, the optical properties of the material usually do not change, so even more drastic adaptations must be made to the reactor design, or the visualization of the process has to be limited to top surface only. Mejia et al. [32] have built a set-up that would allow them to view and record the top particle layers inside the reactor (Fig. 4). The left image shows the top view of a bed of pristine Ca(OH)<sub>2</sub> grains. The middle and right image shows the



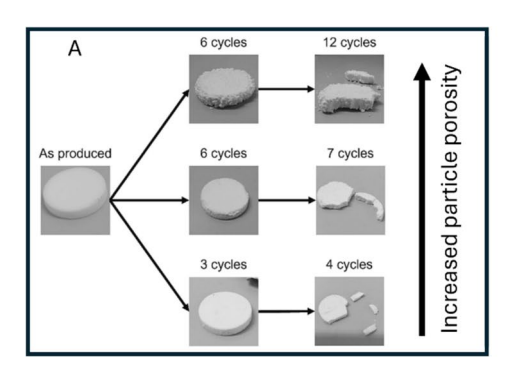
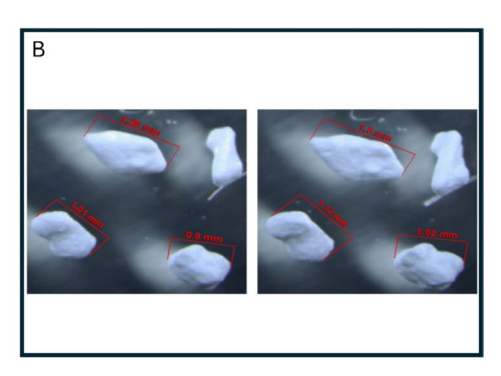


**Fig. 2** Optical images of the degradation of K<sub>2</sub>CO<sub>3</sub> particles with various particle porosities over consecutive (dis)charging cycles (**A**). Adapted from "Impact of cycling on the performance of mmsized salt hydrate particles," by J. Aarts, H. Fischer, O. Adan, and H. Huinink, 2024, Journal of Energy Storage, 76, p. 109806 (https://doi.org/10.1016/j.est.2023.109806). CC BY [27]. Optical images of

same top view after 10 and 20 (dis)charge cycles, respectively. Comparing the start and end situation shows a different bed structure. The thermocouple still visible at the start (grey rod) has been buried in the material after cycling due to expansion of the material.

Such setup allows for easier determination when the physical material degradation starts to occur as the inside of the reactor can be inspected during reaction without disassembly. Nevertheless, it is our experience that the degradation of the particles in the middle or at the bottom of the reactor is much more considerable due to the added compression from all the particles above and no room to expand freely. This means that the surface particles are the best-case scenario. A full glass reactor would give better insight; however, this would lead to high thermal losses due to poor insulation properties of glass and poor performance of the reactor. Even then, the core of the reactor could not be inspected due to outer layers of the material.

Another approach for studying the evolution of particle morphology in a bed-like setting involves a flatbed reactor with single particle layer. When a single layer of particles is confined in a well-defined space, with no excess volume around them, their behavior during reaction will mimic the behavior of a single layer of particles confined by other particles within the reactor. The correlation is not identical, as the particles in the flat bed reactor will not experience the additional weight of the material above it unless pressure is applied with the top plate, but it is still a reasonable approximation to study the interplay between the reactive gas flow pattern, morphological changes in the particles and the feedback loop it can create over a number of cycles as particles deform, fuse and crack. Figure 5A shows how the grey salt particles turn black starting at the bottom (gas inlet). This blackening is due to deliquescence (overhydration) and the salt particles start to dissolve [33].



K<sub>2</sub>CO<sub>3</sub> particles before and after 12 (dis)charging cycles indicating particle swelling (**B**). Adapted from "Effect of cycle-induced crack formation on the hydration behaviour of K2CO3 particles: Experiments and modelling," by M. A. J. M. Beving, A. J. H. Frijns, C. C. M. Rindt, and D. M. J. Smeulders, 2020, Thermochimica Acta, 692, p. 178752 (https://doi.org/10.1016/j.tca.2020.178752). CC BY [28]

By coupling such reactor with a thermal imaging camera (Fig. 5B), the temperature evolution within the particle bed can be tracked. It is visible that especially at the bottom, close to the gas inlet, and top left the fastest temperature increase is observed. At the bottom this is expected due to the inlet of water vapor at this location. However, the fast temperature increase on the top left indicates possible wall channeling of preferential flow path effects.

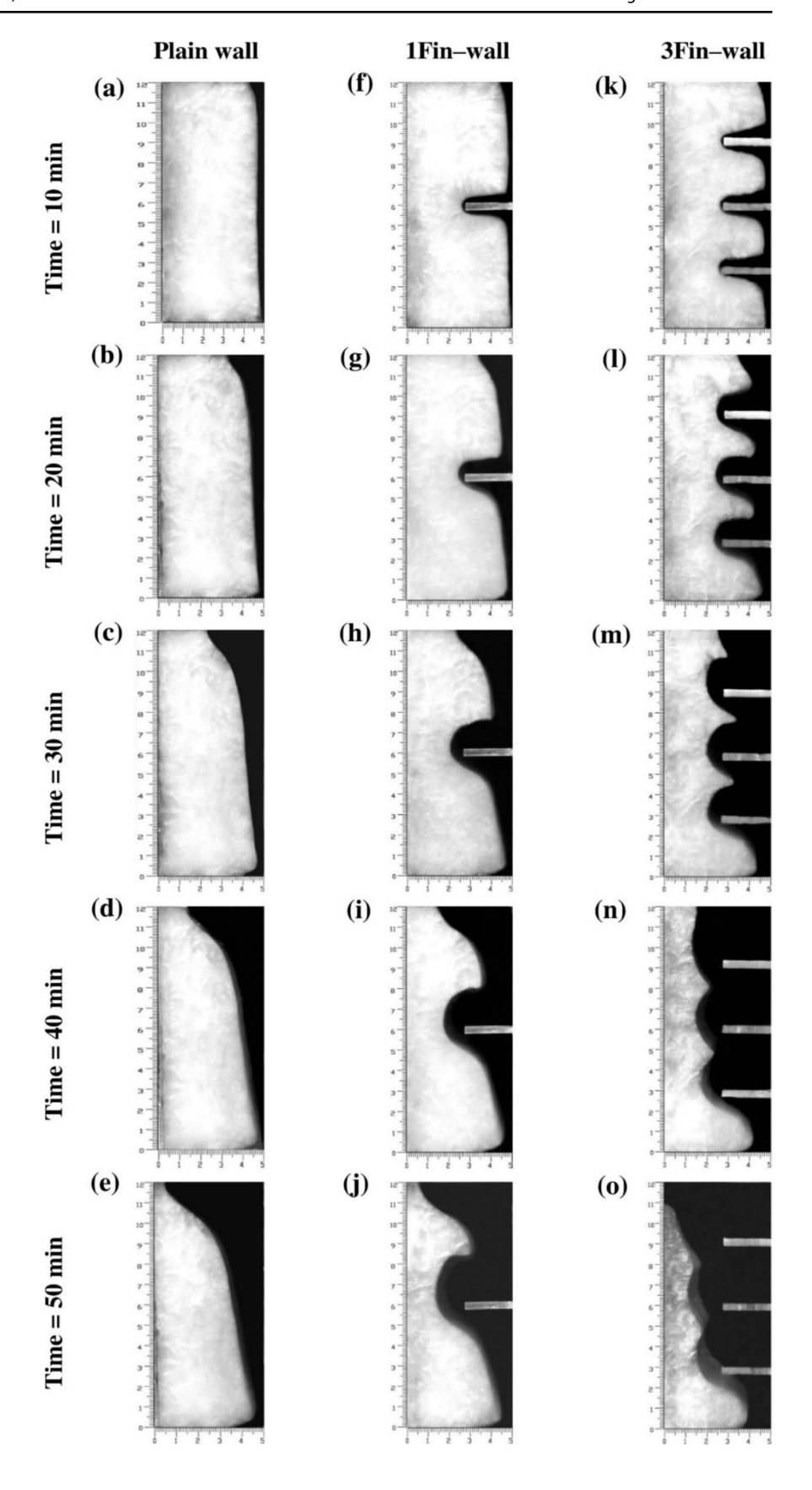
Combining IR and optical imaging adds another layer of information that enables better understanding of the relationship between reaction progress, morphological changes, and flow paths. In general, thermal imaging is a valuable tool in mapping the behavior of various heat storage materials [34, 35].

IR imaging can be also applied to LHS to track the reaction progress as shown in Fig. 6. In their work, Liang et al. (2024) have followed the solidification process of  $Na_2SO_4\cdot 10H_2O$  with different carboxymethyl cellulose (CMC) content (0–10%), to monitor the impact of the thickener on the phase separation of the salt as well as its heat capacity [36]. The authors observed different cooling rates between the different contents of CMC. The sample without any CMC had cooled down completely after 20 min (completely yellow) whereas samples with CMC were able to retain a higher temperature for longer times (red color). Indirectly from this, the latent heat and thermal conductivity could be determined as PCMs with high latent heat will maintain their phase transition temperature for longer.

It is therefore noteworthy to mention that optical techniques are limited to the amount of information that can be derived. As optical imaging can only provide 2D information of the observed layer, mostly being the top or outer surface, the conclusions drawn cannot be generalized to the bulk of the material. The same holds for optical thermal imaging as it only a 2D image is provided without any information in

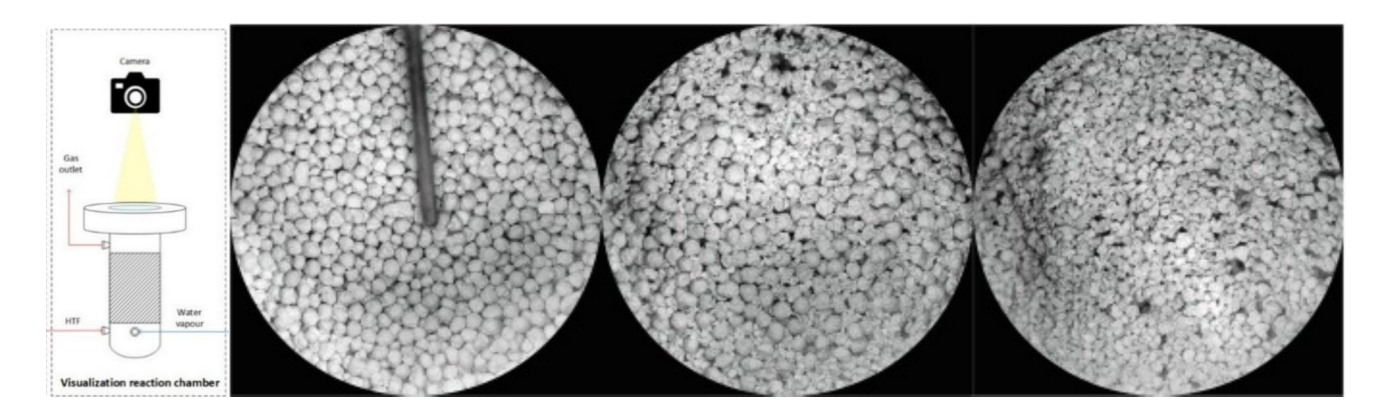


Fig. 3 Photographs of the melting process in the rectangle enclosure with partial fins on the right and without fins at every 10 min while the right wall is maintained at 70 °C. In these photographs, the white and black colors represent the solid and liquid phases of the PCM, respectively. Based on the changes in the solid phase, the dominant heat transfer mechanism, heat transfer rate as well as other processes and forces can be determined. The imaged sample area is 12×5 cm. Reprinted from International Journal of Heat and Mass Transfer, 78, B. Kamkari, and H. Shokouhmand, Experimental investigation of phase change material melting in rectangular enclosures with horizontal partial fins, 839-851., Copyright (2014), with permission from Elsevier [29]





141 Page 6 of 20 Journal of Nondestructive Evaluation (2025) 44:141



**Fig. 4** Schematic of an experimental set up used to monitor the appearance of the top of the reactor during operation (left), followed by the photos taken during the before, during (10 (dis)charge cycles) and after (20 (dis)charge cycles) the cyclic experiment showing the morphological changes at the surface of the bed. The rod visible in the first image is a thermocouple that gets buried in the TCM during

cycling due to material expansion. Adapted from Real-time visualization and experimental analysis of stabilized Ca(OH)2 granules for thermal energy storage," by A. C. Mejia, S. Afflerbach, M. Linder, and M. Schmidt, 2024, Energy Conversion and Management: X, 23, p. 100656 (https://doi.org/10.1016/J.ECMX.2024.100656). CC BY [32]

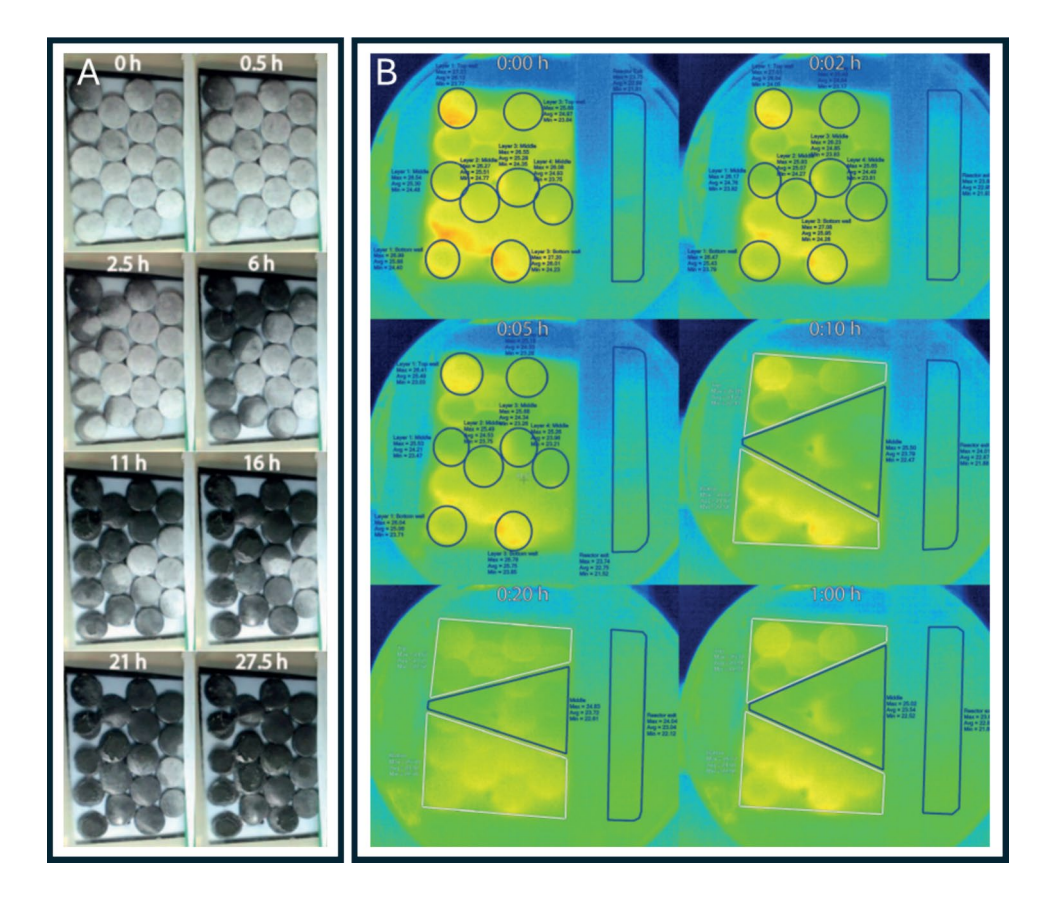


Fig. 5 Optical image of flatbed reactor filled with  $K_2CO_3$  particles during deliquescence (A). A reaction front Is seen during deliquescence of the particles when excess moisture leads to color change. Thermal images of a flatbed reactor filled with  $K_2CO_3$  during (over) hydration (B). The temperature front developed during hydration observed with thermal camera does not lead to significant differences in particle appearance compared to images recorded with a regular optical camera. However, it can be used to monitor reaction and tem-

perature fronts in the reactor bed. Orange areas have higher temperatures than the blue zones. Adapted with permission from "Hydration fronts and particle bed mechanics: Visual studies of thermo-chemical heat storage flat-bed reactors: An experimental physics study of sustainable energy storage," by B. J. A. Van Schaik, 2022, Eindhoven University of Technology. Copyright 2022 by Brandon van Schaik [33]



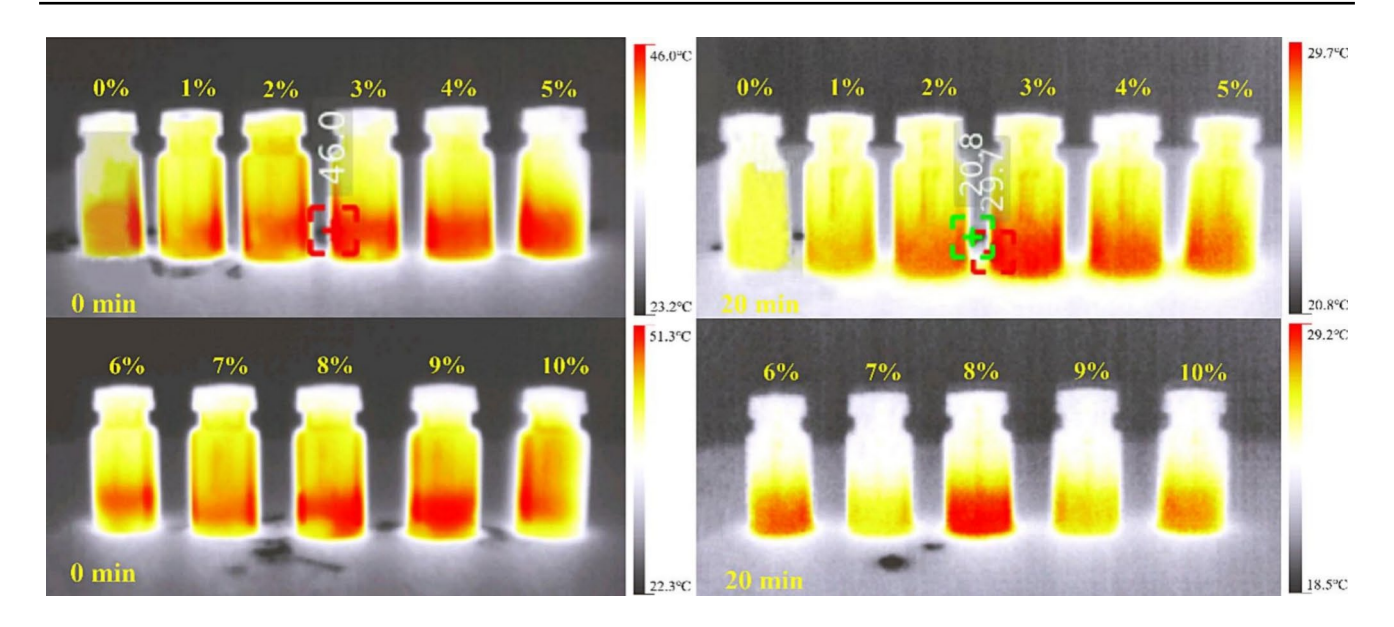


Fig. 6 Na<sub>2</sub>SO<sub>4</sub>·10H<sub>2</sub>O with different CMC mass ratios imaged during cooling with thermal infrared imaging camera at the same time interval. Reprinted from Journal of Energy Storage, 83, Q. Liang, H. Zhang, Y. Li, X. Zhang, and D. Pan, Multifunctional response of

biomass carbon/sodium sulfate decahydrate composite phase change materials, 110621., Copyright (2024), with permission from Elsevier [36]

the direction perpendicular to the imaging plane. Therefore, to get a full understanding of the inside of the heat storage vessel a combination with a 3D technique is required.

### 2.2 Nuclear Magnetic Resonance (NMR)

Nuclear magnetic resonance (NMR) employs the effect a strong magnetic field has on nuclei of atoms. By applying a well-defined magnetic field, the spins of the nuclei, typically randomly arranged, will align with the direction of the field. When the field is turned off, the spins will go back to their original random orientation. The time it takes, the relaxation time, depends on several factors, such as the nature of the element and its environment (other neighboring elements, chemical bonds, environmental conditions, etc.).

The NMR can be used in two different modes. First, NMR spectroscopy, most often applied in chemistry, is used for molecular analysis. NMR spectroscopy is employed for a limited number of nuclei (<sup>1</sup>H, <sup>13</sup>C, <sup>15</sup>N, <sup>19</sup>F, and <sup>31</sup>P) as the nuclei are required to have a spin. The best know examples of NMR spectroscopy are <sup>1</sup>H liquid NMR spectroscopy and <sup>13</sup>C solid state NMR spectroscopy [37, 38]. The basis of NMR spectroscopy relies on the following: In the absence of a magnetic field the magnetic moments of the nuclei are randomly oriented, but as soon as the nuclei are placed in an external magnetic field, the magnetic moments will align with this external field. Most nuclei will align with the magnetic field (lowest energy state) whereas a small number of nuclei will be rotated 180 degrees opposed to the magnetic field (high energy state). Supplying radio frequency (rf)

radiation corresponding to the energy difference between the high and low energy state (resonance frequency) allows the nuclei to flip between the two states. During this process they release a signal which can be detected.

The specific resonance frequency depends on the precise chemical environment and interaction between atoms or molecules.

Secondly, NMR is utilized for imaging studies, which is the main NMR application in the studied works. Here, 1D, 2D and 3D images are created based on the concentration of the exited nuclei at certain positions [39]. Spatial NMR imaging is possible due to the gradient present in the applied magnetic field. Due to this gradient the resonance frequency becomes location dependent which allows for the analysis of the materials divided into different slices. The signal intensity in each slice is given by the following equation [40]

$$S \propto \sum \rho_{\rm H} \exp\left(-\frac{t_{\rm e}}{T_2}\right) \left(1 - \exp\left(-\frac{t_{\rm r}}{T_1}\right)\right)$$
 (1)

Here  $\rho_{\rm H}$  represents the density of the hydrogen protons,  $T_1$  and  $T_2$  represent the longitudinal and transversal relaxation times, respectively, and  $t_{\rm e}$  and  $t_{\rm r}$  represent the echo and repetition time, respectively.

The most well-known example of NMR imaging is medical magnetic resonance imaging (MRI), which used to create live 2D and 3D images of human body parts [41]. However, NMR imaging is also employed in several other fields of interest such as liquid penetration [42], oil and gas industry [43], paintings [44], and geological porous media [45].



Within the domain of heat storage, NMR imaging has been shown to be of value for TCHS and LHS. Within TCHS, NMR imaging is used on both material and reactor level. Donkers et al. (2015, 2015, and 2016) showed how NMR can be used to quantify the water content (hydration levels) in the material as a function of position and provide in-situ structural information [46–48]. As the signal intensity scales with the hydrogen atom density (water molecule density), the total hydration level of the material could be measured as function of time and position [46]. The authors used a Hahn sequence in which they have chosen long  $t_{\rm e}$  times compared to  $T_{\rm 2}$  and short  $t_{\rm r}$  compared to  $T_{\rm 1}$  to maximize the signal intensity (see Eq. 1) [49].

A more sophisticated analysis of the relaxation times can be used to identify the environment of the water molecules and can be related to the structure of the material [48]. Shorter relaxation time is related to crystal water bound in the lattice of the material, whereas longer times are related to for example, pore water [47]. Such analysis, employed by Qiu et al. (2023), enable the authors to identify two states of bound water in silica gels [50]. Again, since the water content directly correlates with the observed signal, the authors could also calculate the total water content in the material using NMR.

On a reactor level, the same type of measurement can be applied. In this case, NMR can be used to monitor water front movement through the bed [23, 51]. The impact of flow conditions (humidity, flow rate, temperature), particle shape and size and packing density can be investigated. Information such as conversion rate, power output and flow distribution can be extracted from the measurements, as exemplified in Fig. 7.

Here the authors used Hahn spin echo measurements to create a 1D image indicating the conversion (loading) at various positions inside a reactor bed of  $K_2\mathrm{CO}_3$  particles. The left-hand side of the image corresponds to the inlet of the packed bed and the profiles from dark green to blue correspond to a measurement interval of 12 h. In the first time profiles, an increase in loading is observed close to the inlet of the reactor bed. At longer times, slowly the loading starts to increase from left to right, indicating a hydration front travelling trough the bed from inlet to outlet.

Nevertheless, NMR techniques, due to relatively poor spatial resolution, will not provide any information about individual particles within the bed or their morphological changes. Employing a 3D NMR technique, as done by Gaeni et al. (2017), which is synonymous with a medical scanner, enables to gather moisture profiles throughout the reactor volume [52]. This makes the observations of for example reactor edge effects more explicit, yet it is not resolved enough to look at individual particles. It provides valuable insight on reactor level, though it cannot be used on scales small enough to gain insight into the fundamental processes

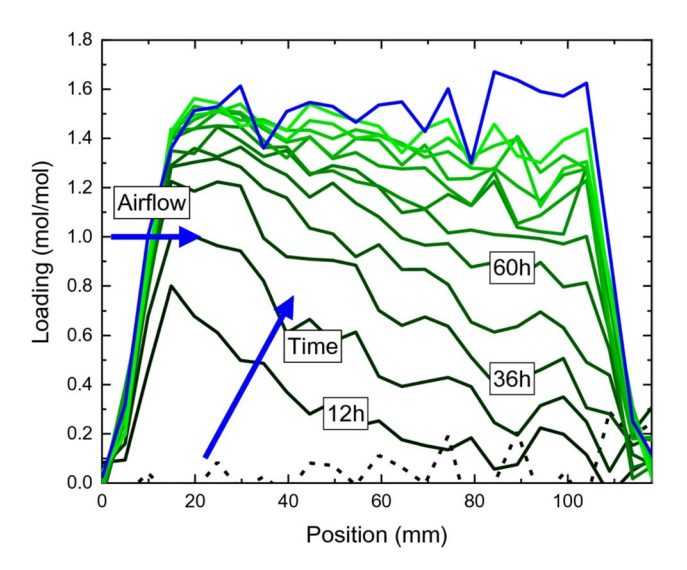


**Fig. 7** Loading (conversion) as a function of position in a reactor bed for various reaction times. The figure shows the evolution of a reaction front throughout the reactor bed and can be used to monitor the evolution of the reaction in-situ. From "Investigation into the Hydration Behaviour of  $K_2CO_3$  Packed Beds: An NMR Study," by T. Raemaekers, P. Donkers, and H. Huinink, 2023, Journal of Energy Storage, 149(3), p. 826 (10.1007/s11242-023–01985-7). CC BY [23]

on particle level. To increase the resolution, the echo time must be increased, however this makes it unable to measure the short relaxation times associated with hydration and crystal water.

Imaging NMR studies can be expanded with Magnetic Resonance Thermometry (tMR) investigation. tMR principles can be used to study a variety of materials [53–55] and several different techniques exist to conduct NMR temperature imaging [56]. The basic principle behind tMR is that parameters such as T1, T2, diffusion constant and chemical shift are affected by changes in temperature, allowing for temperature mapping given the values are known at a reference temperature [57]. The differences and challenges associated with the assorted techniques are beyond the scope of this work.

In case of heat storage applications, additional significant relaxation shifts occur due to solid–liquid phase transition of the material, as the interactions between the molecules change drastically. When several of those effects are closely monitored and coupled during analysis, a detailed phase and temperature map of a material can be made. In LHS, tMR has been used for temperature and phase mapping of encapsulated phase change material (PCM) on particle [58] and bed level [59]. Skuntz et al. (2018) used tMR to map the melt front propagation in a packed bed of PCM particles (Fig. 8) [59]. The authors took 3 longitudinal slices at various times to visualize the melting behavior (conversion) versus time and position. The inflow of hot and inert fluorocarbon-based liquid is placed at the bottom



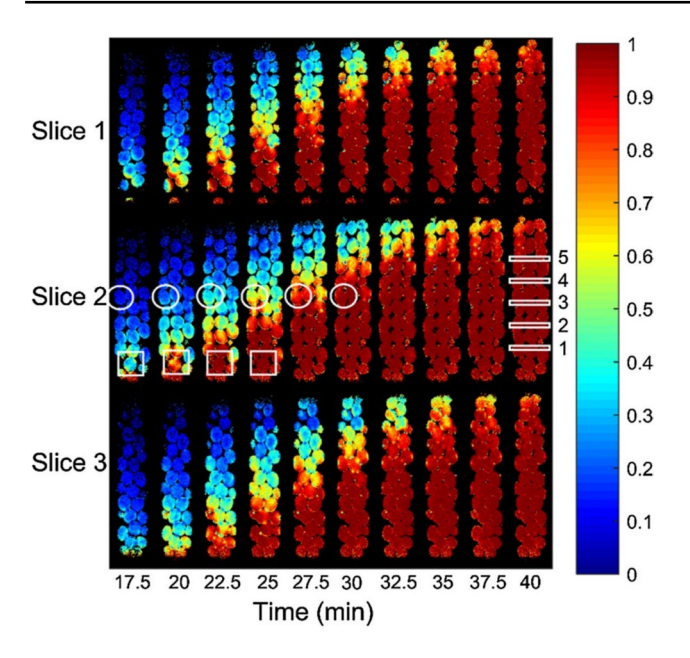


**Fig. 8** Melt front propagation versus time for 3 longitudinal slices. Blue is fully unmolten and red fully molten PCM (scale bar corresponds to conversion). The white circled areas are areas with high longitudinal flow whereas the white squared areas are areas with high transverse flow. The white rectangular boxes labels 1 to 5 are used to construct transversal slices in Fig. 10 of the original work. Reprinted from Chemical Engineering Science, 190, M. E. Skuntz, D. Perera, J. E. Maneval, J. D. Seymour, and R. Anderson, Melt-front propagation and velocity profiles in packed beds of phase-change materials measured by magnetic resonance imaging, 164–172., Copyright (2018), with permission from Elsevier [59]

of the vessel. The melt front propagating from bottom to top is clearly visible as the gradual changes from blue (unmolten) to red (molten) with increasing time, allowing for determination of a melt front and melt front velocity.

Such studies enable the study of the dynamics of melting and solidification processes at different conditions and at different positions within the reactor, down to individual encapsulated particles. Further, the effect of packing and flow of heat transfer fluid around the particles can be studied and potential dead zones identified. Furthermore, the energy transfer process can be also identified and compared with computational data for better understanding of the multitude of processes that simultaneously occur in a heat storage reactor.

An adaptation of this technique, done in the study by Skuntz et al. (2021) in which the heat transfer fluid flow through the bed has also been probed with NMR [60]. It adds a complementary set of data aiding in understanding the heat flow patterns observed in the PCM. It also provides a more holistic approach to studying heat storage reactors where not only the active material is scrutinized but also the fluid that transfers the heat.

### 2.3 Attenuation X-ray Imaging

Similarly to NMR, X-ray imaging is extensively used in medicine from simple cases as broken bones to advanced techniques as 3D imaging of the body with a CT scan [61]. In science, it is widely utilized in a variety of disciplines to image the (micro)structure of various materials such as construction materials [62], batteries [63], archaeological specimens [64], and heat storage materials [65]. Several X-ray imaging modalities exist such as X-ray phase contrast imaging which uses information on the X-ray phase change when passing through a sample [66], X-ray dark field imaging which uses the diffracted X-ray beam leaving the sample to create an image of the interested area [67], and attenuation X-ray imaging which will be the focus of this section.

Attenuation X-ray imaging employs the contrast difference caused by X-ray attenuation and can be classified as a transmission type imaging modality. The X-ray beam generated by a source of choice (most commonly an X-ray tube with a tungsten anode) passes through the imaged object. In the process some of the radiation is attenuated before reaching the detector. Based on the amount of attenuation through the sample, contrast can be generated between areas with high and low X-ray attenuation. The amount of attenuation, which results in visible contrast, depends on multiple factors. First, the atomic number of the imaged material as elements with higher atomic numbers tend to cause more attenuation. Second, the thickness and density of the material affect the total attenuation as thicker or higher material density regions will attenuate the X-ray beam more. Especially when analyzing phase change materials a sufficient density difference between the solid and molten phase must exist [68]. Third, the X-ray energy will affect the attenuation as lower energy X-rays are attenuated more. By adjusting the energy of the beam expressed in kV and the radiation intensity expressed in mAs, an optimal image with good contrast and high signal-to-noise ratio can be obtained [69].

Thanks to the maturity of X-ray imaging technology, 2D imaging techniques based on X-ray attenuation are less popular in latest investigations as they give a single viewpoint of the specimen. Through 3D imaging (computed tomography, CT), a wider range of information can be gathered at the expense of longer imaging time (several minutes up to an hour depending on the exact device [68]). For example, when imaging particle beds, the X-ray tomography images can be used to develop a 3D mesh that replicates the particles and the void between them. Such a computer-generated mesh can be then used to calculate various particle or bed properties, such as density or porosity or even to model gas flow and heat transfer through the imaged volume. An example of such work is the study by Arya et al. (2024). In this work they focused on imaging



particle beds and in particular reactive gas flow through the bed [24]. The authors used micro-CT generated images to create a 3D model and evaluate the changes in bed properties after 10 (dis)charge cycles. Both open and closed porosity, grain size distribution, and percolation paths (Fig. 9) in both packed beds were calculated using GeoDict software with PoreDict, GrainFind, and percolation path function, respectively. These results were used to compute the fluid flow paths using the FlowDict module. Although the use of predefined modules enables easier computation, it lacks information about the assumptions and approximation embedded in these modules.

In Fig. 9 the grey parts represent the salt hydrate whereas the white parts represent the porous void space between the particles. The percolation paths (dark grey lines) represent the connected pores available for vapor transport starting at the colored spheres at the top of the images. In the uncycled (left) bed the percolation paths seem more evenly distributed over the sample volume whereas in the cycled material the percolation paths appear more convoluted. As these percolation paths are crucial for the vapor flow through the packed bed using micro-CT can be used to optimize the structure for efficient use of the bed capacity.

This shows that X-ray tomography is not only a tool for visual inspection of morphological changes but that it is also a starting point for a much more sophisticated analysis. The ability to calculate and visualize flow paths of the reactive

gas through the particle bed and changes in those give invaluable insights on how to better engineer particles, reactor and the gas delivery system. It also enables researchers to follow the changes in the particles as a function of bed depth which is not possible with optical techniques that look solely at the top layer.

With high enough resolution, similar measurement can be conducted on a single particle. The morphological changes of those, such as particle swelling and cracking are relatively easy to image [70]. By imaging a single particle through a number of cycles, the development of internal porosity in single TCM particle can be readily followed with micro-CT [65]. Such data can be then used to correlate the development in internal porosity network, increase in particle volume and enhancement in reaction kinetics.

The impact of particle coating, focus of many investigations on TCMs [71–73], was also studied with micro-CT by Elahi et al. [74]. Thanks to the high resolution of the technique, not only the thermochemical material, but also the coating (polyether sulfone (PES)) itself could be imaged (Fig. 10). The authors were able to clearly distinguish between the salt hydrate (orange) and coating (blue). Such works give insights into coating properties such as thickness, porosity, and interfacial properties between particle and coating as well as the grain structure of the particle. The porous nature of the coating (Fig. 10B) can be clearly linked to the SEM image of the top surface of

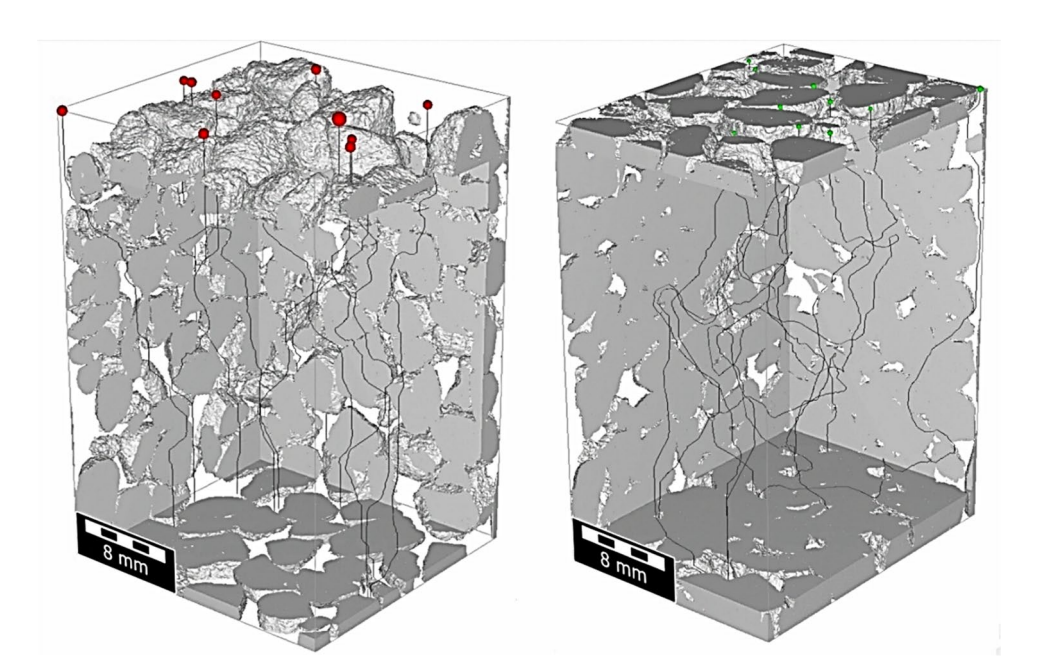
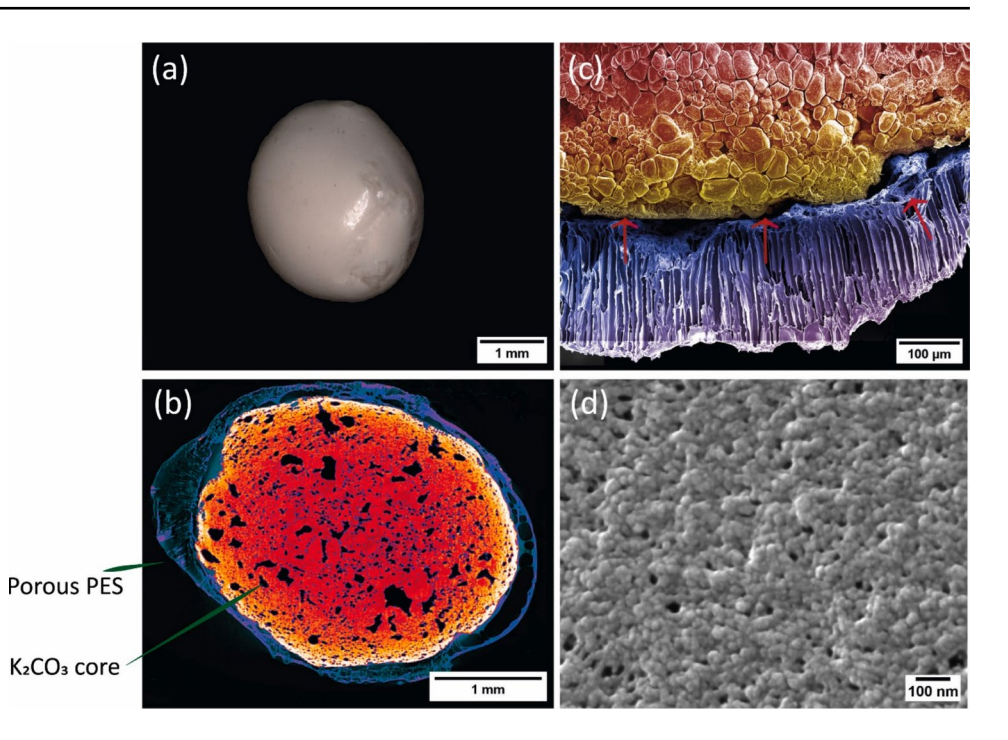


**Fig. 9** Percolation paths obtained from CT data in an uncycled (left) and cycled (right) TCM particle bed which can be used to the fluid flow in both systems. The grey parts represent the salt hydrate whereas the white parts represent the porous void space in between the particles. The percolation paths (dark grey lines) represent the connected pores available for vapor transport starting at the col-

oured spheres at the top of the images. Adapted from "Characterizing Changes in a Salt Hydrate Bed Using Micro X-ray Computed Tomography," by A. Arya, J. Martinez-Garcia, P. Schuetz, A. Mahmoudi, G. Brem, P. A. J. Donkers, and M. Shahi, 2024, Journal of Nondestructive Evaluation, 43(3), p. 77 (10.1007/s10921-024–01092-7). CC BY [24]



Fig. 10 K<sub>2</sub>CO<sub>3</sub> macrocapsule morphology images: one macrocapsule particle (a), Micro-CT cross-section (b), SEM interface image of porous PES coating and K2CO3 granule (c), and top surface PES coating layer SEM image (d). From "Boosting stability of K2CO3 granules for thermochemical heat storage applications through innovative membrane encapsulation," by B. Elahi, D. Salehzadeh, W. Vos, N. Shahidzadeh, G. Brem, and M. Mehrali, 2024, Chemical Engineering Journal, 500, p. 157042 (10.1016/j. cej.2024.1570427). CC BY [74]



the coating (Fig. 10D) showing nanometer sized holes in between the grain structure of the coating layer. This shows how Micro-CT and SEM imaging can serve as complimentary techniques.

Several works focusing on LHS have employed X-ray CT to monitor melting fronts and crystallization behavior of various materials [75–78]. Thanks to the density differences between solid and liquid phase, reaction fronts can be precisely followed (Fig. 11) [79]. This allows for calculating reaction speeds, degree of conversion and indirectly, temperature distribution in the material.

Additionally, the liquid fraction during the melting and solidification can be precisely determined. Figure 11a shows the melting of ice as a function of time. Using X-ray CT exact liquid fraction can be derived and coupled with a numerical model. For an in-depth discussion the reader is referred to Guarda et al. [80].

The work from which Fig. 11b originates also serves as a clear example of why collecting 3D information is so important compared to 2D imaging. When looking at the 2D snapshots taken from the full tomography, the reaction progress can be easily monitored. However, 2D images do not provide in depth resolved information. For example, in Fig. 11b solidification of CaCl<sub>2</sub>·6H<sub>2</sub>O is observed. However, based on those images it is impossible to tell with complete certainty whether the crystallization of the needle shaped particle visible in the middle of the vial starts in the bulk of the material or if one of the edges touches the wall of the vial.

When the original 3D images obtained from X-ray CT (3D rendering) are provided, the exact growth of the crystals

over time is visible in more detail (Fig. 12) [79]. It is now clearly visible that crystal growth starts at the edges and bottom of the container followed by the fusion of these crystals growing inwards (towards the center) of the container [81]. This illustrates the key difference in detail which can be obtained from 2 and 3D images.

### 2.4 Neutron Imaging

Neutrons, just like X-rays, can be used for diffraction and imaging studies. Neutron diffraction has been used to analyze various materials such as crystalline proteins [82] and single crystals [83]. Neutron imaging is a technique complimentary to X-ray imaging. The main principle of neutron imaging is like X-ray imaging in the sense that it uses the attenuation properties of the imaged object. The main difference with X-ray imaging is that X-rays interact with the electron clouds of elements whereas neutron interact with the atomic nucleus. Therefore, in contrast to X-ray imaging, many lighter elements exhibit high attenuation coefficients for neutrons while exhibiting low attenuation coefficients for X-rays.

Hydrogen is one of the elements with high attenuation coefficient, making hydrogen-rich materials, such as water, prime candidates for imaging with neutrons. The main difference with NMR, also suitable for imaging high hydrogen content materials, is that NMR relies on the excitation of hydrogen in contrast to the physical interaction neutrons have. This means that in comparison to X-ray imaging, the contrast in the image is more closely related to the chemical



141 Page 12 of 20 Journal of Nondestructive Evaluation (2025) 44:141

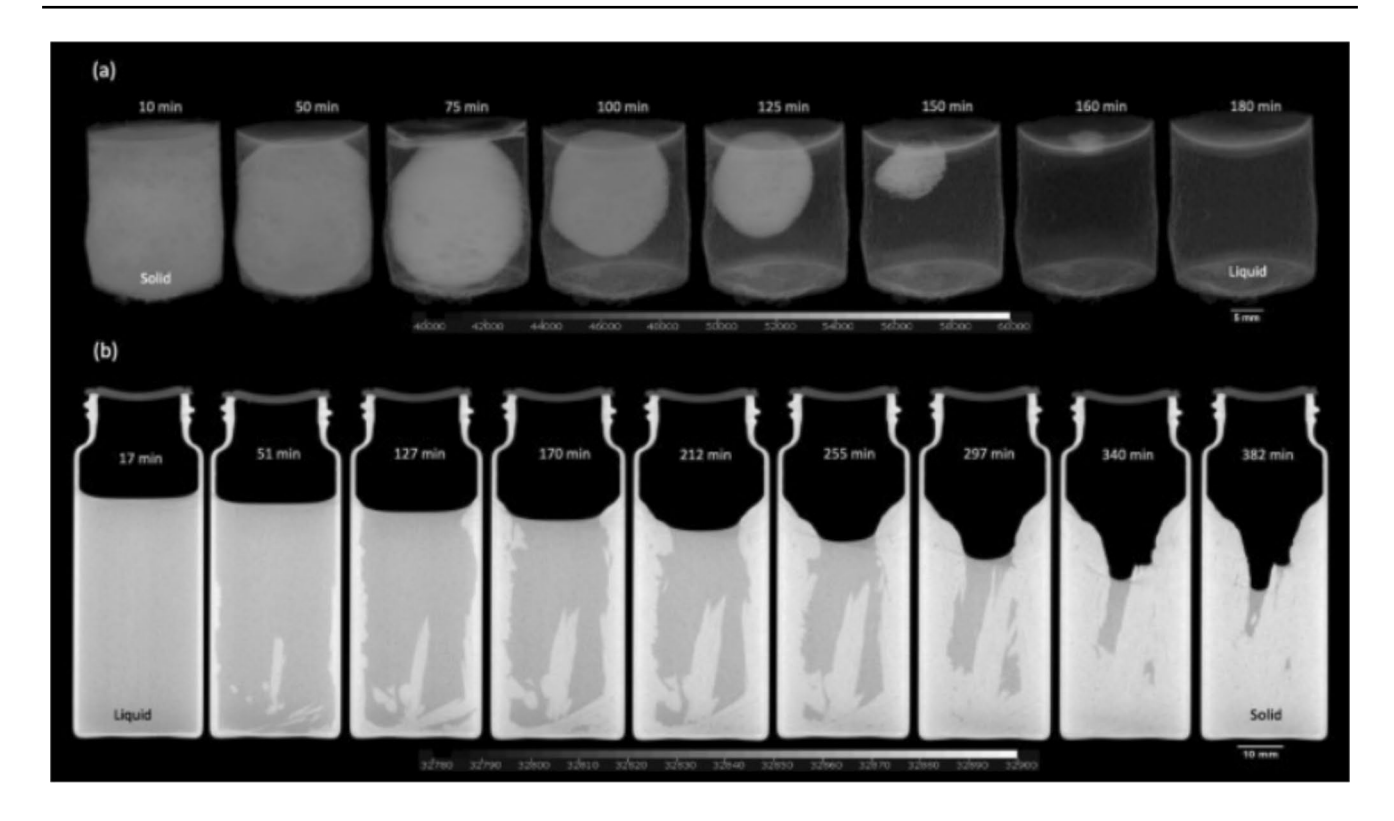


**Fig. 11** Melting of Ice (a) and 2D snapshots of the solidification of calcium chloride hexahydrate (b) using 3D rendered CT images. From "Volumetric quantification of melting and solidification of phase change materials by in-situ X-ray computed tomography," by J.

Martinez-Garcia, D. Gwerder, F. Wahli, D. Guarda, B. Fenk, A. Stamatiou, J. Worlitschek, and P. Schuetz, 2023, Journal of Energy Storage, 61, p. 106726 (10.1016/J.EST.2023.106726). CC BY [79]

make-up of the sample and not its physical density. In addition, neutrons can be used to investigate the nanoporous structure of materials using small-angle neutron scattering (SANS) [84].

Neutron imaging has been applied in a wide range of fields [85]. In energy related topics, it is more commonly used in visualizing water transport in fuel cells and to image electrical batteries [86] as lithium has high attenuation coefficient [87]. In case of heat storage, it has been employed only to visualize processes occurring in TCHS with ammonia or water as reactive gas [25].

In the work conducted by Berdiyeva et al. (2020),  $NH_3$  sorption and material expansion into the reactor was followed through series of 2D images taken during reaction. This technique allowed authors to monitor  $NH_3$  absorption and material expansion at selected reaction conditions and position within the reactor compared to the starting value (white dashed line) (Fig. 13).

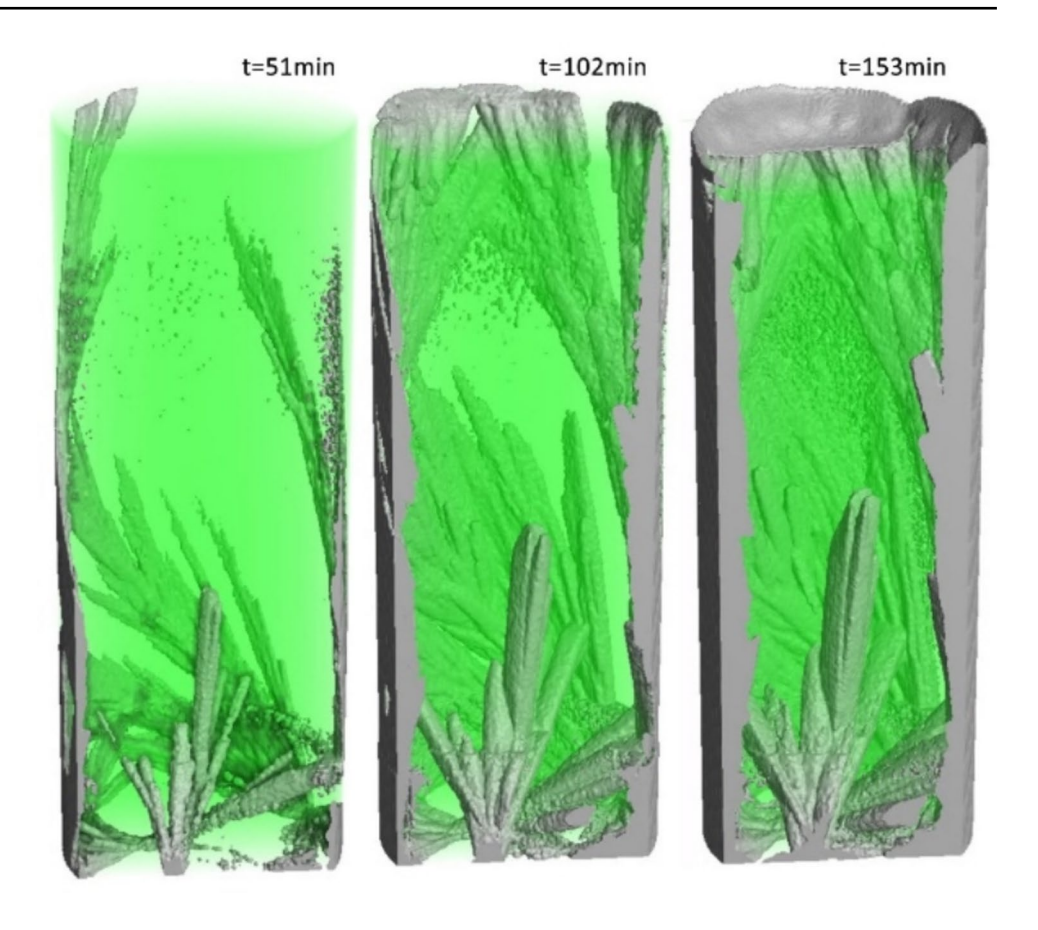
Similar to NMR, by evaluating the changes in the signal attenuation, in this case  $NH_3$  content as a function of time, reaction progress can be precisely quantified and related to degree of conversion. This information was used as an input for modelling, similarly to the previously described MRI study on  $K_2CO_3$  [52], and eventually a better reactor

design. Furthermore, material movement within the reactor, as shown in Fig. 13, could be visualized. This again can be used as input for reactor design and operation to accommodate the morphological changes. By monitoring the conversion rate within the reactor, inhomogeneities or even dead zones in the gas or heat supply can be identified and rectified with better design. Furthermore, by following expansion or shrinkage of the material, the points where material reorganization leads to loss of thermal contact to the heat exchanged can be detected. Both inhomogeneities in heat and gas flow can have limited impact for compact systems, however the severity of such effects will compound in larger systems. Thus, it is crucial for large scale applications that they are identified and rectified in advance.

Similar to those investigations, transport of water vapor into  $\rm K_2\rm CO_3$  particles can be readily imaged. The advantage of using neutron imaging is that apart from structural changes, clear hydration fronts for water absorption can be visualized with good contrast as well in a single experiment. An example of new results provided in this work shown in Figs. 14 and 15. In this example, neutron imaging was performed at the Paul Scherrer Institute (PSI) in Switzerland at the ICON beamline. Neutrons are generated using a spallation neutron source at PSI after which they are moderated



Fig. 12 Semitransparent 3D rendering of crystal formation (grey regions) at different times. Green regions represent the liquid PCM phase. Adapted from "Volumetric quantification of melting and solidification of phase change materials by in-situ X-ray computed tomography," by J. Martinez-Garcia, D. Gwerder, F. Wahli, D. Guarda, B. Fenk, A. Stamatiou, J. Worlitschek, and P. Schuetz, 2023, Journal of Energy Storage, 61, p. 106726 (10.1016/J. EST.2023.106726). CC BY [79]



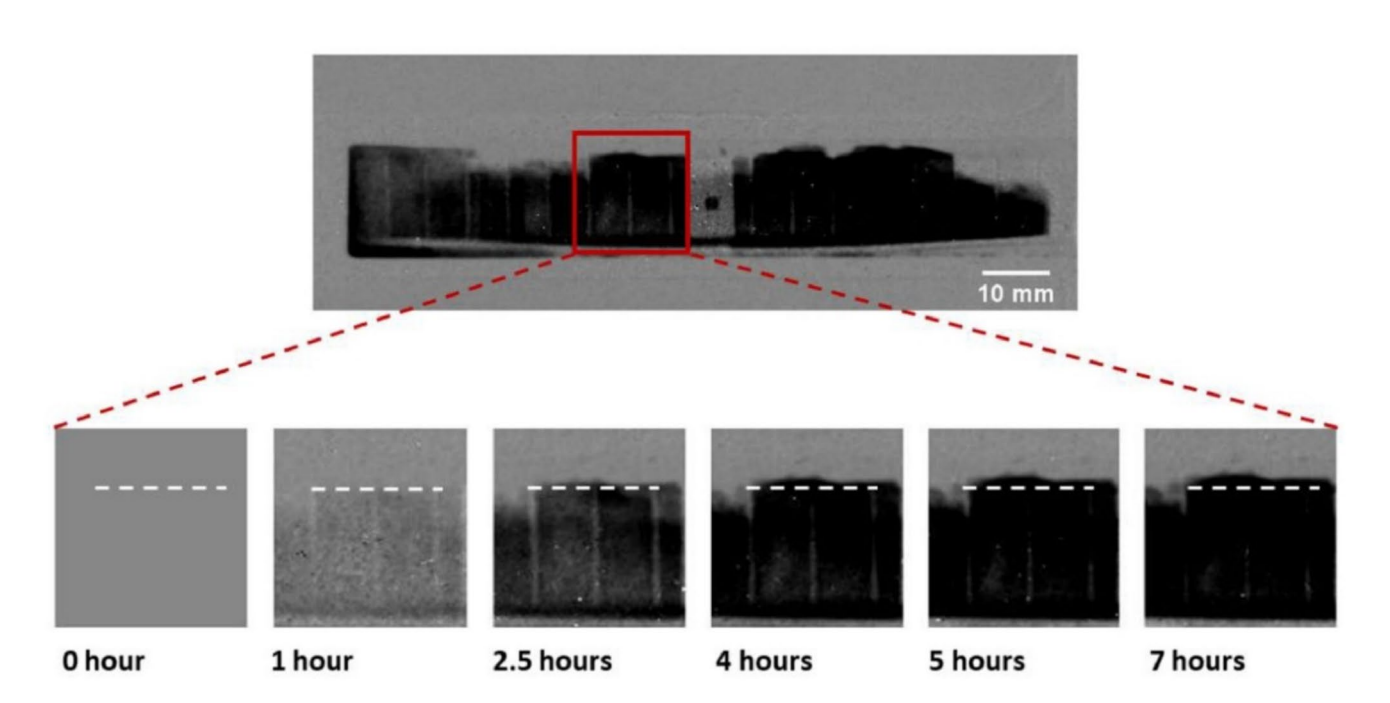


Fig. 13 Conversion and expansion during  $NH_3$  absorption by  $SrCl_2$  at various reaction times inside a selected region within the reactor. From "In-situ neutron imaging study of  $NH_3$  absorption and desorption in  $SrCl_2$  within a heat storage prototype reactor," by P. Berdiyeva,

A. Karabanova, M. G. Makowska, R. E. Johnsen, D. Blanchard, B. C. Hauback, and S. Deledda, 2020, Journal of Energy Storage, 29, p. 101388 (https://doi.org/10.1016/J.EST.2020.101388). CC BY [25]



141 Page 14 of 20 Journal of Nondestructive Evaluation (2025) 44:141

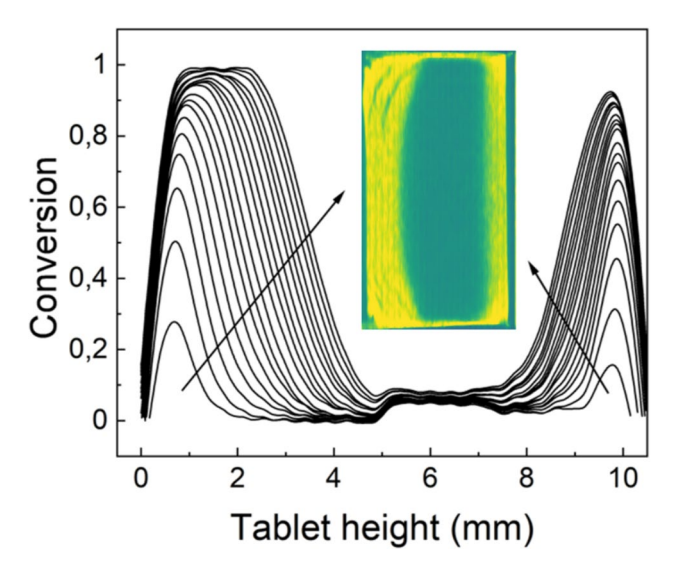


Fig. 14 Progress of hydration (conversion) over time at different tablet heights calculated from differences in neutron attenuation between anhydrous (green) and hydrated (yellow) material. The insert shows a 2D image of the  $K_2CO_3$  particle towards the end of the experiment. Yellow colour indicates high attenuation coefficient caused by water absorption and formation of  $K_2CO_3 *1.5H_2O$  while the green colour indicates low attenuation coefficient of anhydrous material. Arrows point towards the progress in the reaction. The profiles were collected every 30 min

using liquid deuterium at 25 K. For a detailed instrumental description, the reader is referred to Kaestner et al. (2011) [88]. Projections were collected using Golden-Ratio Decomposition [89].

For analysis, the samples are placed within aluminium containers which are transparent for the neutrons. This was done to prevent interaction between the surrounding atmosphere and the sample. The sample was exposed to two water sources with different humidity, resulting in two reaction fronts within the particle. Those reaction fronts are shown in form of yellow coloring in the insert (Fig. 14).

The plot shown in Fig. 14 is similar to the reaction fronts that can be obtained with NMR shown in Fig. 7. In Fig. 7 the conversion over time over the reactor length is given whereas in Fig. 14 the same information is given for a single particle. This shows that neutron imaging allows individual particles to be measured. Given that the exact sample properties and the reaction conditions are known, the diffusion constant of the single particle can be extracted and compared with previously published values [90, 91]. Furthermore, morphological changes can be monitored and correlated to the conversion degree, conversion rate or particle shape.

From application point of view, studying a packed bed reactor, as the one shown in Fig. 15, is more interesting. Such experiments, executed in the same experimental setup as Fig. 14, now equipped with advective controlled humidity, can clearly show reaction front development in time through the reactor volume. Furthermore, it shows that the particles react from outside in (as expected), however close proximity between some particles hampers the water uptake in some cases, leaving unreacted (dark) cores at the end of the measurement (Fig. 15B). Moreover, cracks and deformation can be observed in some particles (Fig. 15B and D). This means that a more careful image analysis could reveal changes in particle volume, leading to change in porosity and gas flow paths through the reactor, similarly to X-ray CT [24, 65]. Note that in Fig. 15 beam hardening effects can be seen as a higher intensity at the particle edges facing outwards of the sample. As the detailed explanation is beyond the scope of this work the reader is referred to the following references for a detailed explanation [92, 93]

The reverse reaction, dehydration, can also be studied. This means that the relationships between particle shape, size packing and vapor/heat supply can be resolved in much greater detail than when using only classical pressure drop measurements. This clearly pinpoints where the issues in the reactor occur and enables much more efficient progress in the system design. Last, similarly to X-ray CT, data collected

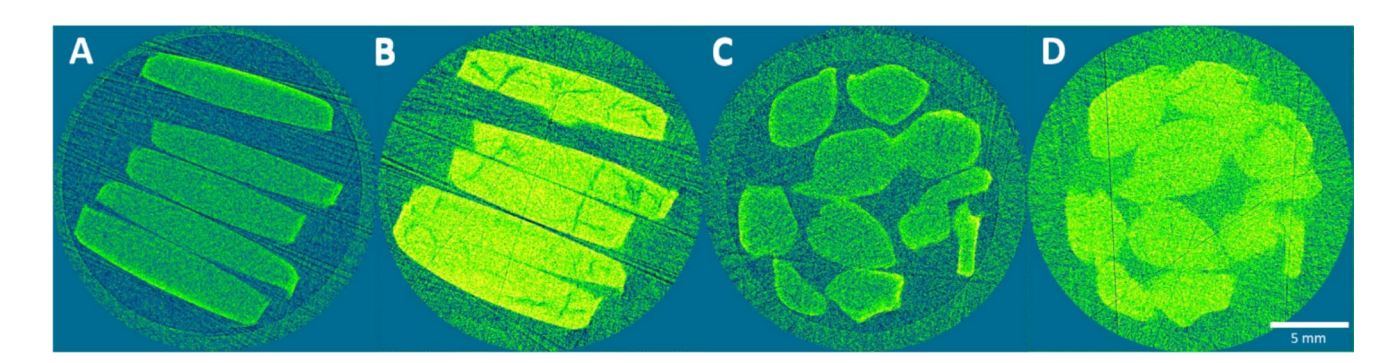


Fig. 15 Selected slices of neutron tomograms taken from the middle of a reactor before (A and C) and during (B and D) K<sub>2</sub>CO<sub>3</sub> packed bed hydration. The use of different particle shapes show how packing efficiency can avvect energy and power density



through neutron imaging can be used to generate 3D models and to study gas flow through the bed.

Finally, neutron imaging has been utilized to visualize processes in light metal hydrides [94–96]. Although the focus of those works was hydrogen storage, the same thermochemical reaction (M+n/2  $H_2=MH_n$ ) can be utilized for heat storage, as  $H_2$  absorption is reversible and exothermic [97]. Comparably to water based thermochemical storage, the storage temperature depends on partial pressure of hydrogen and varies from room temperature to several hundred degrees Celsius. Hydrogenation of light metal hydrides suffers from similar challenges as hydration of salt hydrates, thus the ability to follow the reaction progress throughout the material is of great value.

# 2.5 Other NDT Techniques that could be of Advantage to Heat Storage Applications

In the sections above, we have presented a series of NDT techniques that have been utilized on number of occasions to investigate various heat storage systems. In this section, we'll provide a summary of NDT techniques that has not been applied to the best of our knowledge, but that we believe could be of use in this field of research.

Scanning acoustic microscopy (SAM) uses focused sound waves to image an object. It is commonly used to visualize defects within material and to conduct failure analysis. In the energy storage field, it has been used to investigate various aspects of lithium batteries such as electrode aging, or casing damage [98]. It is a useful technique for detecting impurities and cracks, often used in combination with X-ray tomography. In nuclear power plants, it has been used for in-situ diagnosis and monitoring of corrosion of the molten-salt reactor [99]. Such work could be potentially applied to sensible heat storage reactors using water or molten salts.

Positron Emission Tomography (PET) imaging is another technique commonly used in medicine and other fields of science but not utilized in heat storage. It utilizes radioactive substances to monitor their location, concentration and movement, if for example injected into blood flow. Jing et.al. has utilized this technique to investigate the process of CO<sub>2</sub> geo-sequestration [100]. To do so, they generate [<sup>11</sup>C] CO<sub>2</sub> radioisotope and directly inject it into their CO<sub>2</sub> sorbent samples. The reaction mechanism is comparable with sorption based thermochemical storage. Commonly, water vapor is used as reactive gas and CO<sub>2</sub> as an impurity, when for example zeolites are considered as a heat storage material. Nevertheless, there are certain thermochemical reactions that utilize CO<sub>2</sub> as the reactive gas, where this technique could be more applicable [101–103].

### 2.6 Comparison of Techniques

### 2.6.1 Imaging in 2D or 3D

As mentioned at the start of Sect. 2, many of the abovementioned techniques, and in particular NMR, X-rays and neutrons, can be used to generate both 2D and 3D images. The advantage of taking 2D images is shorter imaging time which might facilitate following the processes in near real time. Depending on the technique, it takes less than one minute to collect a single image. Higher quality images require longer exposure times to improve the signal to noise ratio, however if the reaction progress is sufficiently slow this might not have significant impact on the collected data. Unfortunately, 2D images typically give an accumulated composition in the view direction. This means that they tend to be an average of the imaged volume or a snapshot at certain depth within the material or provide surface information. It also means that assumptions must be made regarding the uniformness of the observed phenomenon in other directions. If samples are uniform and symmetrical, such assumptions are readily made, but in many cases the properties of the sample vary throughout the volume, making the observations less precise and incomplete information is obtained.

By integrating a range of images at different angles we can obtain a 3D volume representation. This means that such data can be used to look at both the entire volume and at selected 2D slices. However, in this case, the viewpoint of the 2D images can be selected after the measurement and readily be changed depending on the interest. Nevertheless, such images will be compounded by an imaging sequence that can take from several minutes to more than half an hour. It means that it is in general not suitable for fast processes, as effects of those will get lost due to the necessary image integration in postprocessing. It must be noted that some techniques are available which generate 3D images in a faster manner such as using synchrotron radiation [104]. For this, the golden ratio acquisition method can be used which sacrifices spatial resolution in favor of temporal resolution [89]. Further, the generation of 3D images is more expensive computationally and timewise, compared to 2D image analysis. However, if such work is done well, it can be used as input for further modelling work, as demonstrated before.

The key benefits and drawbacks of 2D and 3D imaging techniques are summarized in Table 1.

### 2.6.2 Comparison of Imaging Modalities

As mentioned in Sect. 2.2, many of the techniques are complementary to each other. In particular, neutron and X-ray imaging are often used in tandem [105]. This is because neutrons interact very well with organic materials (due to



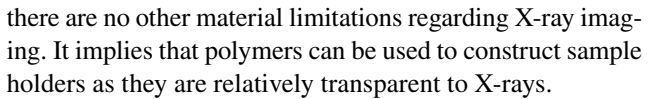
Table 1 Benefits and drawbacks of using 2D and 3D imaging techniques

	Benefit	Drawback
2D	Fast More accessible Can give near life view of a reaction	Images as average of the volume Single viewpoint Requires several assumptions dur- ing analysis
3D	Full view of the process Can give 2D images from any viewpoint	Time consuming post processing Sensitive to gradual changes dur- ing the scan Requires sophisticated detector and/or processing software

high H concentration) which are semi-transparent in X-ray due to low density and amorphous nature. On the other hand, heavier elements tend to be opaque in X-ray and more transparent in neutron. This enables to obtain two drastically different images. NMR imaging falls between the two other techniques as the primary contrast comes from differences in proton density and the chemical nature of the imaged object, similarly to neutron imaging, but it does not have equal penetration depth.

NMR imaging is a mature technology enabling both 2D and 3D visualization of various objects. It is relatively accessible, and it uses non-ionizing radiation (magnetic fields and radio waves). As mentioned, it relies on the concentration of specific nuclei and it is not suitable for dense materials, which somewhat limits its applicability in science and engineering. Furthermore, the main disadvantage of this technique is its inability to image samples that can be permanently magnetized or that are encapsulated in material that can be permanently magnetized or that has a high density of protons. This means that samples that are inserted into NMR cannot be placed in a metal vessel, as this would be attracted by the magnetic field. Also, most common polymers cannot be used for vessel construction due to their high H-concentration that would overshadow any material placed inside. Most commonly, glass or PTFE sample holders are utilized as they will not disturb the signal or provide additional background noise. This unfortunately puts significant constraints on the vessel design, resulting in only relatively small reactors being imaged.

X-ray imaging is a further mature technology used for both 2D and 3D imaging studies. It is highly available compared to other techniques considered, with the advanced setups providing resolution of tens of nanometers (nano-CT). It is ideal for imaging dense materials; however, the ionizing radiation might pose issues to for example biobased material. A possible downside to using X-rays is that X-rays can affect the wettability of certain materials during the measurement, possibly affecting the results [106]. Besides that,



In some cases, for X-ray, NMR and neutron imaging, contrast agents can be used to further enhance image quality. Such agents are then more sensitive towards the chosen technique than the rest of the sample, thus showing up more clearly during imaging. Contrast agents for X-rays can be used to better visualize flow patterns through the material or highlight areas of interest through absorption [107, 108]. In many cases, the contrast agents do not chemically interact with the sample, and they can be fully removed after the experiment. For NMR imaging, metallic particles, such as Fe<sub>2</sub>O<sub>4</sub> could be utilized as iron strongly interacts with magnetic fields. Nevertheless, many other options are possible, depending on the final application [109]. For Neutron imaging liquid gadolinium contrast agents can be used. For example, in crack detection these gadolinium compounds can penetrate the cracks enhancing their visibility [110, 111].

Finally, neutron imaging can be used to obtain complementary data to X-ray or NMR. However, because it requires access to specialized facilities, it presents limited use in the wider scientific and industrial community. In addition, the spatial resolution is lower, and acquisition times are longer compared to X-ray CT. It has a great penetration depth and resolution of 10–100 um. Although, in principle, any material could be imaged using neutron beams, many do become radioactive after exposure, making them impossible to handle without potential associated health risks. Finally, with greatest contrast provided by light elements, the variety of applications is somewhat limited by the chemical composition of the material. Aluminium has been shown to be an ideal material for sample vessels as it is transparent in neutron beams and its activation decays quickly. Polymers are not suitable due to their high hydrogen concentration, but any parts made from organic material can be easily picked up in the imaging process.

### 3 Conclusion

The understanding of processes in heat storage materials and reactors can be greatly improved using non-destructive methods that allow a view inside the objects. The advantage of non-destructive methods is that the sample remains intact, experimental changes can be monitored in-situ, and the experiments are less labor intensive. Three most utilized non-destructive techniques for heat storage systems are NMR, X-ray imaging, and neutron imaging.

NMR can be used to characterize both TCES and LHS systems. When investigating TCES systems, NMR can only provide information on the overall reactor as the spatial



resolution is too low for identification of individual particles, whereas on the other hand in LHS systems employing tMR, individual particles in the reactor can be distinguished as well. NMR and tMR are therefore best suited for imaging samples for which structural information is less important.

X-ray imaging is a suitable method for investigating the structural evolution in TCES and LHS reactors. Individual particles can be imaged as well due to the higher spatial resolution compared to NMR. X-rays can be successfully used to probe the conversion in these systems due to the density difference between the charged and discharged states.

A suitable addition to X-ray imaging is neutron imaging as it relies on the hydrogen content of the sample. In a TCES system, the contrast between charged and discharged material can be the highest as the charged (dry) material mostly does not contain any hydrogen atoms. The images of TCES systems obtained from X-ray and neutron imaging can be superimposed providing full structural and conversion information of the sample. The downside of the technique is that it is relatively expensive, only small sample sizes can be used.

Which technique to use greatly depends on the required information and sample characteristics. Whereas spatial resolution improves in the order of NMR < neutrons < X-rays, the experimental difficulty increases in the order of NMR < X-rays < Neutrons, resulting in a trade-off between the desired information and available resources.

Nevertheless, it should be remembered that the gauge volume changes with the resolution. When very fine resolution is desired, typically only a small volume can be imaged, thus limiting the experimental scope. However, as each technique provides unique information about the sample combining multiple techniques, such as for example neutron tomography and thermal imaging, is desired for a full understanding of the heat storage system. Only by overlaying several data sources can a complete picture of such complex system be obtained.

**Acknowledgements** Parts of this work is based on experiments performed at the Swiss spallation neutron source SINQ, Paul Scherrer Institute, Villigen, Switzerland. Therefore, they are gratefully acknowledged.

**Author Contributions** J.A and N.M wrote the main manuscript text. A.K and H.F were responsible for supervision and guidance during the experimental work at PSI. A.K and H.F were responsible for acquiring beamtime at PSI. All authors reviewed and edited the manuscript. All authors performed the new experiments presented in this work.

**Funding** This publication is part of the Mat4Heat project with project number 739.017.014 of the research program Mat4Sus which is financed by the Dutch Research Council (NWO).

**Data Availability** Should any raw data files be needed in another format as present in this work they are available from the corresponding author upon reasonable request.

#### **Declarations**

Competing interests The authors declare no competing interests.

**Open Access** This article is licensed under a Creative Commons Attribution 4.0 International License, which permits use, sharing, adaptation, distribution and reproduction in any medium or format, as long as you give appropriate credit to the original author(s) and the source, provide a link to the Creative Commons licence, and indicate if changes were made. The images or other third party material in this article are included in the article's Creative Commons licence, unless indicated otherwise in a credit line to the material. If material is not included in the article's Creative Commons licence and your intended use is not permitted by statutory regulation or exceeds the permitted use, you will need to obtain permission directly from the copyright holder. To view a copy of this licence, visit http://creativecommons.org/licenses/by/4.0/.

### References

- "Delivering the European Green Deal." Accessed: Oct. 02, 2023. [Online]. Available: https://commission.europa.eu/strat egy-and-policy/priorities-2019-2024/european-green-deal/ delivering-european-green-deal\_en
- 2. IEA, "Heating." Accessed: Sep. 29, 2023. [Online]. Available: https://www.iea.org/energy-system/buildings/heating
- 3. Mertens, S.: Design of wind and solar energy supply, to match energy demand. Clean. Eng. Technol. **6**, 100402 (2022). https://doi.org/10.1016/j.clet.2022.100402
- Hasrat, I.R., Jensen, P.G., Larsen, K.G., Srba, J.: Modelling of Hot Water Buffer Tank and Mixing Loop for an Intelligent Heat Pump Control, in *Lecture Notes in Computer Science* (including subseries Lecture Notes in Artificial Intelligence and Lecture Notes in Bioinformatics), vol. 14290 LNCS, 2023, pp. 113–130. https://doi.org/10.1007/978-3-031-43681-9\_7
- Pereira da Cunha, J., Eames, P.: Thermal energy storage for low and medium temperature applications using phase change materials – A review. Appl. Energy 177, 227–238 (2016). https://doi.org/10.1016/j.apenergy.2016.05.097
- Tatsidjodoung, P., Le Pierrès, N., Luo, L.: A review of potential materials for thermal energy storage in building applications. Renew. Sustain. Energy Rev. 18, 327–349 (2013). https://doi. org/10.1016/j.rser.2012.10.025
- Nonnen, T., et al.: A thermochemical long-term heat storage system based on a salt/zeolite composite. Chem. Eng. Technol. 39(12), 2427–2434 (2016). https://doi.org/10.1002/ceat.201600301
- Michel, B., Mazet, N., Mauran, S., Stitou, D., Xu, J.: Thermochemical process for seasonal storage of solar energy: characterization and modeling of a high density reactive bed. Energy 47(1), 553–563 (2012). https://doi.org/10.1016/j.energy.2012.09.029
- Farid, M.M., Khudhair, A.M., Razack, S.A.K., Al-Hallaj, S.: A review on phase change energy storage: materials and applications. Energy Convers. Manag. 45(9–10), 1597–1615 (2004). https://doi.org/10.1016/j.enconman.2003.09.015
- 10 Kant, K., Shukla, A., Smeulders, D.M.J., Rindt, C.C.M.: Performance analysis of a K2CO3-based thermochemical energy storage system using a honeycomb structured heat exchanger. J. Energy Storage 38(March), 102563 (2021). https://doi.org/10.1016/j.est.2021.102563
- Mahmoudi, A., Donkers, P.A.J., Walayat, K., Peters, B., Shahi, M.: A thorough investigation of thermochemical heat storage system from particle to bed scale. Chem. Eng. Sci. 246, 116877 (2021). https://doi.org/10.1016/j.ces.2021.116877



- Pitié, F., Zhao, C.Y., Baeyens, J., Degrève, J., Zhang, H.L.: Circulating fluidized bed heat recovery/storage and its potential to use coated phase-change-material (PCM) particles. Appl. Energy 109, 505–513 (2013). https://doi.org/10.1016/j.apenergy.2012.12.048
- Bouhal, T., Fertahi, S., Agrouaz, Y., El Rhafiki, T., Kousksou, T., Jamil, A.: Numerical modeling and optimization of thermal stratification in solar hot water storage tanks for domestic applications: CFD study. Sol. Energy 157, 441–455 (2017). https://doi.org/10.1016/j.solener.2017.08.061
- Andersen, E., Furbo, S., Hampel, M., Heidemann, W., Müller-Steinhagen, H.: Investigations on stratification devices for hot water heat stores. Int. J. Energy Res. 32(3), 255–263 (2008). https://doi.org/10.1002/er.1345
- Kumar, K., Singh, S.: Investigating thermal stratification in a vertical hot water storage tank under multiple transient operations. Energy Rep. 7, 7186–7199 (2021). https://doi.org/10. 1016/j.egyr.2021.10.088
- Hao, C., Feng, G., Ma, C., Barreneche, C., She, X.: Performance analysis of a novel multi-module columnar packed bed reactor with salt hydrates for thermochemical heat storage. J. Energy Storage 86, 111170 (2024). https://doi.org/10.1016/j.est.2024.111170
- Kumar, K., Singh, S.: Investigating thermal stratification in a hot water storage tank during charging mode. J. Phys. Conf. Ser. 2178(1), 012001 (2022). https://doi.org/10.1088/1742-6596/ 2178/1/012001
- Huinink, H., de Jong, S., Houben, V.: Hydration fronts in packed particle beds of salt hydrates: implications for heat storage. J. Energy Storage 71, 108158 (2023). https://doi.org/10.1016/j.est. 2023.108158
- Akademia Baru, P., et al.: A Review on Application of Non Destructive Techniques on Composites. J. Adv. Res. Appl. Mech. 20(1), 12–21, 2016, Accessed: Aug. 30, 2024. [Online]. Available: https://www.akademiabaru.com/submit/index.php/aram/article/view/1752
- Sposito, G., Ward, C., Cawley, P., Nagy, P.B., Scruby, C.: A review of non-destructive techniques for the detection of creep damage in power plant steels. NDT E Int. 43(7), 555–567 (2010). https://doi.org/10.1016/J.NDTEINT.2010.05.012
- Silva, M.I., Malitckii, E., Santos, T.G., Vilaça, P.: Review of conventional and advanced non-destructive testing techniques for detection and characterization of small-scale defects. Prog. Mater. Sci. 138, 101155 (2023). https://doi.org/10.1016/J. PMATSCI.2023.101155
- Dwivedi, S.K., Vishwakarma, M., Soni, P.A.: Advances and researches on non destructive testing: a review. Mater. Today Proc. 5(2), 3690–3698 (2018). https://doi.org/10.1016/J.MATPR. 2017.11.620
- Raemaekers, T., Donkers, P., Huinink, H.: Investigation into the hydration behavior of K2CO3 packed beds: an NMR study. Transp. Porous Media 149(3), 817–835 (2023). https://doi.org/ 10.1007/s11242-023-01985-7
- Arya, A., et al.: Characterizing changes in a salt hydrate bed using micro X-ray computed tomography. J. Nondestr. Eval. 43(3), 77 (2024). https://doi.org/10.1007/s10921-024-01092-7
- Berdiyeva, P., et al.: In-situ neutron imaging study of NH3 absorption and desorption in SrCl2 within a heat storage prototype reactor. J. Energy Storage 29, 101388 (2020). https://doi. org/10.1016/J.EST.2020.101388
- Tan, P., Lindberg, P., Eichler, K., Löveryd, P., Johansson, P., Kalagasidis, A.S.: Effect of phase separation and supercooling on the storage capacity in a commercial latent heat thermal energy storage: experimental cycling of a salt hydrate PCM. J. Energy Storage 29, 101266 (2020). https://doi.org/10.1016/j.est.2020.101266
- Aarts, J., Fischer, H., Adan, O., Huinink, H.: Impact of cycling on the performance of mm-sized salt hydrate particles. J. Energy Storage 76, 109806 (2024). https://doi.org/10.1016/j.est.2023.109806

- 28 Beving, M.A.J.M., Frijns, A.J.H., Rindt, C.C.M., Smeulders, D.M.J.: "Effect of cycle-induced crack formation on the hydration behaviour of K2CO3 particles: Experiments and modelling. Thermochim Acta 692(March), 178752 (2020). https://doi.org/10.1016/j.tca.2020.178752
- Kamkari, B., Shokouhmand, H.: Experimental investigation of phase change material melting in rectangular enclosures with horizontal partial fins. Int. J. Heat Mass Transf. 78, 839–851 (2014). https://doi.org/10.1016/J.IJHEATMASSTRANSFER.2014.07.056
- Guo, J., Li, Z., Xie, Y., Gao, J., Yang, X., Li, M.J.: Improved phase change performance of ultrasonic-assisted melting: a visualized experimental study. Energy 306, 132500 (2024). https:// doi.org/10.1016/J.ENERGY.2024.132500
- Kunkel, S., et al.: Channel formation and visualization of melting and crystallization behaviors in direct-contact latent heat storage systems. Int. J. Energy Res. 44(6), 5017–5025 (2020). https://doi. org/10.1002/ER.5202
- Cosquillo Mejia, A., Afflerbach, S., Linder, M., Schmidt, M.: Real-time visualization and experimental analysis of stabilized Ca(OH)2 granules for thermal energy storage. Energy Convers. Manage.: X 23, 100656 (2024). https://doi.org/10.1016/J.ECMX. 2024.100656
- Van Schaik, B.J.A.: Identifying the hydration front and other reactor mechanics a thermo-chemical heat storage flat-bed reactor via visual methods, Eindhoven University of Technology, (2022)
- Garai, A., Kleissl, J., Llewellyn Smith, S.G.: Estimation of biomass heat storage using thermal infrared imagery: application to a walnut orchard. Boundary-Layer Meteorol. 137, 333–342 (2010). https://doi.org/10.1007/s10546-010-9524-x
- Jarenwattananon, N.N., et al.: Thermal maps of gases in heterogeneous reactions. Nature 502(7472), 537–540 (2013). https://doi.org/10.1038/nature12568
- Liang, Q., Zhang, H., Li, Y., Zhang, X., Pan, D.: Multifunctional response of biomass carbon/sodium sulfate decahydrate composite phase change materials. J. Energy Storage 83, 110621 (2024). https://doi.org/10.1016/j.est.2024.110621
- van de Velde, F., Knutsen, S.H., Usov, A.I., Rollema, H.S., Cerezo, A.S.: 1H and 13C high resolution NMR spectroscopy of carrageenans: application in research and industry. Trends Food Sci. Technol. 13(3), 73–92 (2002). https://doi.org/10.1016/S0924-2244(02)00066-3
- Wawer, I., Witkowski, S.: Analysis of solid state 13C NMR Spectra of biologically active compounds. Curr. Org. Chem. 5(10), 987–999 (2001). https://doi.org/10.2174/1385272013374905
- Gupta, A., Stait-Gardner, T., Price, W.S.: NMR imaging and diffusion. Adsorption 27, 503–533 (2021). https://doi.org/10.1007/s10450-021-00298-9
- Brown, R.W., Cheng, Y.-C. N., Mark, E., Haacke, M.R.: Thompson, and Ramesh. Venkatesan, *Magnetic resonances*. John Wiley & Sons, Inc., 2014.
- Cleary, J.O.S.H., Guimarães, A.R.: Magnetic Resonance Imaging, in *Pathobiology of Human Disease*, Elsevier, 2014, pp. 3987–4004. https://doi.org/10.1016/B978-0-12-386456-7. 07609-7
- Nicasy, R.J.K., Waldner, C., Erich, S.J.F., Adan, O.C.G., Hirn, U., Huinink, H.P.: Liquid uptake in porous cellulose sheets studied with UFI-NMR: penetration, swelling and air displacement. Carbohydr. Polym. 326, 121615 (2024). https://doi.org/10. 1016/J.CARBPOL.2023.121615
- Elsayed, M., et al.: A review on the applications of nuclear magnetic resonance (NMR) in the oil and gas industry: laboratory and field-scale measurements. J. Pet. Explor. Prod. Technol. 12, 2747–2784 (2022). https://doi.org/10.1007/s13202-022-01476-3
- Presciutti, F., et al.: Noninvasive nuclear magnetic resonance profiling of painting layers. Appl. Phys. Lett. 93(3), 33505 (2008). https://doi.org/10.1063/1.2963026/321705



- Codd, S.L., et al.: NMR relaxation measurements of biofouling in model and geological porous media. Org. Geochem. 42(8), 965–971 (2011). https://doi.org/10.1016/J.ORGGEOCHEM.2011.03.014
- Donkers, P.A.J., Linnow, K., Pel, L., Steiger, M., Adan, O.C.G.: Na<sub>2</sub>SO<sub>4</sub>·10H<sub>2</sub>O dehydration in view of thermal storage. Chem. Eng. Sci. 134, 360–366 (2015). https://doi.org/10.1016/j.ces. 2015.05.028
- Donkers, P.A.J., Pel, L., Adan, O.C.G.: Experimental studies for the cyclability of salt hydrates for thermochemical heat storage. J. Energy Storage 5, 25–32 (2016). https://doi.org/10.1016/j.est. 2015.11.005
- Donkers, P.A.J., Beckert, S., Pel, L., Stallmach, F., Steiger, M., Adan, O.C.G.: Water transport in MgSO 4 ·7H 2 O during dehydration in view of thermal storage. J. Phys. Chem. C 119(52), 28711–28720 (2015). https://doi.org/10.1021/acs.jpcc.5b08730
- 49. Hahn, E.L.: Spin echoes. Phys. Rev. **80**, 580–594 (1950)
- 50 Qiu, Y., et al.: Thermochemical energy storage using silica gel: Thermal storage performance and nonisothermal kinetic analysis. Solar Energy Mater. Solar Cells **251**(December 2022), 112153 (2023). https://doi.org/10.1016/j.solmat.2022.112153
- Houben. Jelle, "Accelerating thermochemical energy storage by doping," PhD Thesis, Eindhoven University of Technology, 2023. Accessed: Aug. 30, 2024. [Online]. Available: https://resea rch.tue.nl/en/publications/accelerating-thermochemical-energystorage-by-doping
- Gaeini, M., Wind, R., Donkers, P.A.J., Zondag, H.A., Rindt, C.C.M.: Development of a validated 2D model for flow, moisture and heat transport in a packed bed reactor using MRI experiment and a lab-scale reactor setup. Int. J. Heat Mass Transf. 113, 1116–1129 (2017). https://doi.org/10.1016/j.ijheatmasstransfer. 2017.06.034
- Ishihara, Y., et al.: A precise and fast temperature mapping using water proton chemical shift. Magn. Reson. Med. 34(6), 814–823 (1995). https://doi.org/10.1002/MRM.1910340606
- Kuroda, K.: Non-invasive MR thermography using the water proton chemical shift. Int. J. Hyperthermia 21(6), 547–560 (2005). https://doi.org/10.1080/02656730500204495
- Stroud, J., Hankiewicz, J.H., Camley, R.E., Celinski, Z.: On the optimization of imaging parameters for magnetic resonance imaging thermometry using magnetic microparticles. J. Magn. Reson. 333, 107108 (2021). https://doi.org/10.1016/J.JMR.2021.107108
- Quesson, B., De Zwart, J.A., Moonen, C.T.W., Magnetic resonance temperature imaging for guidance of thermotherapy. 2000. https://doi.org/10.1002/1522-2586(200010)12:4
- Webb, A.G.: Temperature measurements using nuclear magnetic resonance," in *Annual Reports on NMR Spectroscopy*, vol. 45, Academic Press, 2002, pp. 1–67. https://doi.org/10.1016/S0066-4103(02)45009-0
- Skuntz, M.E., Anderson, R., Codd, S.L., Seymour, J.D.: Temperature mapping using combined T2 and diffusion weighted MRI of encapsulated phase change materials. Appl. Magn. Reson. 54(11–12), 1589–1605 (2023). https://doi.org/10.1007/s00723-023-01555-6
- Skuntz, M.E., Perera, D., Maneval, J.E., Seymour, J.D., Anderson, R.: Melt-front propagation and velocity profiles in packed beds of phase-change materials measured by magnetic resonance imaging. Chem. Eng. Sci. 190, 164–172 (2018). https://doi.org/10.1016/j.ces.2018.06.019
- Skuntz, M.E., Seymour, J.D., Anderson, R.: Observation of heat transfer due to variable thermophysical properties of sub-, nearand super- critical fluids in porous media by magnetic resonance imaging. Int. Commun. Heat Mass Transf. 128, 105635 (2021). https://doi.org/10.1016/j.icheatmasstransfer.2021.105635
- Duvauferrier, R., et al.: Current role of CT and whole body MRI in multiple myeloma. Diagn. Interv. Imaging 94(2), 169–183 (2013). https://doi.org/10.1016/J.DIII.2012.12.001

- du Plessis, A., Boshoff, W.P.: A review of X-ray computed tomography of concrete and asphalt construction materials. Constr. Build. Mater. 199, 637–651 (2019). https://doi.org/10.1016/j. conbuildmat.2018.12.049
- Yu, Z., Shan, H., Zhong, Y., Zhang, X., Hong, G.: Leveraging advanced x-ray imaging for sustainable battery design. ACS Energy Lett. 7(9), 3151–3176 (2022). https://doi.org/10.1021/ ACSENERGYLETT.2C01297/ASSET/IMAGES/LARGE/ NZ2C01297 0015.JPEG
- Machado, A.S., et al.: Archeological ceramic artifacts characterization through computed microtomography and X-ray fluorescence. X-Ray Spectrom. 46(5), 427–434 (2017). https://doi.org/10.1002/XRS.2786
- Arya, A., Mahmoudi, A., Donkers, P.A.J., Brem, G., Shahi, M.: Microstructural changes in thermochemical heat storage material over cycles: insights from micro-X-ray computed tomography. Renew. Energy 223, 120045 (2024). https://doi.org/10.1016/J. RENENE.2024.120045
- Endrizzi, M.: X-ray phase-contrast imaging. Nucl. Instrum. Methods Phys. Res. A 878, 88–98 (2018). https://doi.org/10. 1016/j.nima.2017.07.036
- Kutsal, M., et al.: The ESRF dark-field x-ray microscope at ID06.
   IOP Conf. Ser. Mater. Sci. Eng. 580(1), 012007 (2019). https://doi.org/10.1088/1757-899X/580/1/012007
- Martinez-Garcia, J., et al.: Applications of X-ray computed tomography technology to solid-liquid phase change materials a review. Energies 18(17), 4704 (2025). https://doi.org/10.3390/ en18174704
- Schueler, B.A.: Clinical applications of basic x-ray physics principles. Radiographics 18(3), 731–744 (1998). https://doi.org/10.1148/radiographics.18.3.9599394
- Salehzadeh, D., Elahi, B., ten Elshof, J.E., Brem, G., Mehrali, M.: Porous potassium carbonate granules with enhanced diffusion kinetics for thermochemical heat storage. Chem. Eng. J. 497, 154560 (2024). https://doi.org/10.1016/J.CEJ.2024.154560
- A. Barsk, M. R. Yazdani, A. Kankkunen, and A. Seppälä, "Exceptionally high energy storage density for seasonal thermochemical energy storage by encapsulation of calcium chloride into hydrophobic nanosilica capsules," *Solar Energy Materials* and *Solar Cells*, vol. 251, no. December 2022, p. 112154, Mar. 2023, https://doi.org/10.1016/j.solmat.2022.112154.
- van Ravensteijn, B.G.P., et al.: Encapsulation of salt hydrates by polymer coatings for low-temperature heat storage applications. ACS Appl. Polym. Mater. 3(4), 1712–1726 (2021). https://doi. org/10.1021/acsapm.0c01186
- Gaeini, M., Rouws, A.L., Salari, J.W.O., Zondag, H.A., Rindt, C.C.M.: Characterization of microencapsulated and impregnated porous host materials based on calcium chloride for thermochemical energy storage. Appl. Energy 212, 1165–1177 (2018). https://doi.org/10.1016/j.apenergy.2017.12.131
- Elahi, B., Salehzadeh, D., de Vos, W.M., Shahidzadeh, N., Brem, G., Mehrali, M.: Boosting stability of K2CO3 granules for thermochemical heat storage applications through innovative membrane encapsulation. Chem. Eng. J. 500, 157042 (2024). https:// doi.org/10.1016/j.cej.2024.157042
- Fenk, B., et al.: Characterization of hydration levels of salt hydrate using X-ray computed tomography. J. Phys. Conf. Ser. (2024). https://doi.org/10.1088/1742-6596/2766/1/012230
- Kohler, T., Kögl, T., Müller, K.: Study of the crystallization and melting behavior of a latent heat storage by computed tomography. Chem. Ing. Tech. 90(3), 366–371 (2018). https://doi.org/10. 1002/CITE.201700096
- Guarda, D., et al.: X-ray computed tomography analysis of calcium chloride hexahydrate solidification. Appl. Therm. Eng. 252, 123618 (2024). https://doi.org/10.1016/J.APPLTHERMALENG. 2024.123618



- Guarda, D.: Analysis of the crystallization and melting processes of phase change materials via X-ray computed tomography, 2024, Accessed: Sep. 04, 2024. [Online]. Available: https://www.resea rch.unipd.it/handle/11577/3513022
- Martinez-Garcia, J., et al.: Volumetric quantification of melting and solidification of phase change materials by in-situ X-ray computed tomography. J. Energy Storage 61, 106726 (2023). https://doi.org/10.1016/J.EST.2023.106726
- Guarda, D., et al.: Phase change material numerical simulation: enthalpy-porosity model validation against liquid fraction data from an X-ray computed tomography measurement/system. Nondestruct. Test. Eval. 37(5), 508–518 (2022). https://doi.org/10. 1080/10589759.2022.2070164
- Martinez-Garcia, J., et al.: Study of the solidification behaviour of phase change materials by in-situ X-ray computed tomography. Res. Rev. J. Nondestructive Test. 1(1), (2023). https://doi. org/10.58286/28164
- Wlodawer, A.: Neutron diffraction of crystalline proteins. Prog. Biophys. Mol. Biol. 40, 115–159 (1982). https://doi.org/10.1016/ 0079-6107(82)90012-8
- Artioli, G.: Single-crystal neutron diffraction. Eur. J. Mineral. 14(2), 233–239 (2002). https://doi.org/10.1127/0935-1221/2002/ 0014-0233
- 84. Zhang, M., Ke, Y., Yang, L., Zhao, P., Zhu, H., Li, Y.: The influence of SC-CO2 on the Nanopore structures of different types of shales based on small-angle neutron scattering and multifractal methods. Energy Fuels 38(15), 14514–14525 (2024). https://doi.org/10.1021/ACS.ENERGYFUELS.4C02972/ASSET/IMAGES/LARGE/EF4C02972\_0010.JPEG
- 85. "Neutron imaging | IAEA." Accessed: Sep. 06, 2024. [Online]. Available: https://www.iaea.org/topics/neutron-imaging
- Ziesche, R.F., Kardjilov, N., Kockelmann, W., Brett, D.J.L., Shearing, P.R.: Neutron imaging of lithium batteries. Joule 6(1), 35–52 (2022). https://doi.org/10.1016/J.JOULE.2021.12.007
- Paul Sherrer Institute, "Attenuation coefficients with neutrons." Accessed: Sep. 06, 2024. [Online]. Available: https://www.psi.ch/en/niag/links
- 88. Kaestner, A.P., et al.: The ICON beamline a facility for cold neutron imaging at SINQ. Nucl. Instrum. Methods Phys. Res. A **659**(1), 387–393 (2011). https://doi.org/10.1016/j.nima.2011.08.022
- Kaestner, A., Münch, B., Trtik, P.: Spatiotemporal computed tomography of dynamic processes. Opt. Eng. 50(12), 123201 (2011). https://doi.org/10.1117/1.3660298
- 90 Aarts, J., et al.: "Diffusion limited hydration kinetics of millimeter sized salt hydrate particles for thermochemical heat storage. J. Energy Storage 47(November 2021), 103554 (2022). https://doi.org/10.1016/j.est.2021.103554
- Cotti, M., Fischer, H., Adan, O., Huinink, H.: A scaling rule for power output of salt hydrate tablets for thermochemical energy storage. J. Energy Storage 87, 111395 (2024). https://doi.org/10. 1016/J.EST.2024.111395
- Vontobel, P., Lehmann, E.H., Hassanein, R., Frei, G.: Neutron tomography: method and applications. Phys. B Condens. Matter 385–386, 475–480 (2006). https://doi.org/10.1016/j.physb.2006.05.252
- Zawisky, M., Bastürk, M., Rehacek, J., Hradil, Z.: Neutron tomographic investigations of boron-alloyed steels. J. Nucl. Mater. 327(2–3), 188–193 (2004). https://doi.org/10.1016/j.jnucmat. 2004.02.011
- Herbrig, K., et al.: Investigations of the structural stability of metal hydride composites by in-situ neutron imaging. J. Power. Sources 293, 109–118 (2015). https://doi.org/10.1016/J.JPOWS OUR.2015.05.039
- Börries, S., et al.: Optimization and comprehensive characterization of metal hydride based hydrogen storage systems using insitu neutron radiography. J. Power. Sources 328, 567–577 (2016). https://doi.org/10.1016/J.JPOWSOUR.2016.08.040

- Pohlmann, C., et al.: In operando visualization of hydride-graphite composites during cyclic hydrogenation by high-resolution neutron imaging. J. Power. Sources 277, 360–369 (2015). https://doi.org/10.1016/J.JPOWSOUR.2014.12.011
- Modi, P., Aguey-Zinsou, K.F.: Room temperature metal hydrides for stationary and heat storage applications: a review. Front. Energy Res. 9, 616115 (2021). https://doi.org/10.3389/FENRG. 2021.616115
- 98. Pitta Bauermann, L., Münch, J., Kroll, M., Enghardt, S., Vetter, M.: Nondestructive defect detection in battery pouch cells: a comparative study of scanning acoustic microscopy and X-ray computed tomography. Energy Technol. 11(12), 2300323 (2023). https://doi.org/10.1002/ENTE.202300323
- Findikoglu, A.T., Droessler, J.E., Chlistunoff, J., Goff, G.S.: Noninvasive, in situ acoustic diagnosis and monitoring of corrosion in molten-salt systems. Corrosion 75(10), 1230–1236 (2019). https://doi.org/10.5006/3253
- 100. Jing, Y., et al.: Positron emission tomography dataset of [11C]carbon dioxide storage in coal for geo-sequestration application. Sci. Data (2023). https://doi.org/10.1038/ S41597-023-02754-3
- Pan, Z.H., Zhao, C.Y.: Gas-solid thermochemical heat storage reactors for high-temperature applications. Energy 130, 155–173 (2017). https://doi.org/10.1016/J.ENERGY.2017.04.102
- 102. Shkatulov, A.I., Kim, S.T., Miura, H., Kato, Y., Aristov, Y.I.: Adapting the MgO-CO2 working pair for thermochemical energy storage by doping with salts. Energy Convers. Manage. 185, 473–481 (2019). https://doi.org/10.1016/J.ENCONMAN. 2019.01.056
- André, L., Abanades, S., Flamant, G.: Screening of thermochemical systems based on solid-gas reversible reactions for high temperature solar thermal energy storage. Renew. Sustain. Energy Rev. 64, 703–715 (2016). https://doi.org/10.1016/J.RSER.2016.06.043
- 104. Vavřík, D., Jakůbek, J., Kumpova, I., Pichotka, M.: Laboratory based study of dynamical processes by 4D X-ray CT with subsecond temporal resolution. J. Instrum. 12(02), C02010 (2017). https://doi.org/10.1088/1748-0221/12/02/C02010
- Mannes, D., Schmid, F., Frey, J., Schmidt-Ott, K., Lehmann, E.: Combined neutron and x-ray imaging for non-invasive investigations of cultural heritage objects. Phys. Procedia 69, 653–660 (2015). https://doi.org/10.1016/J.PHPRO.2015.07.092
- 106. Kwon, Y.B., Weon, B.M., Won, K.H., Je, J.H., Hwu, Y., Margaritondo, G.: X-ray-induced changes in wettability. Langmuir 25(4), 1927–1929 (2009). https://doi.org/10.1021/LA804081K/ASSET/IMAGES/LARGE/LA-2008-04081K\_0002.JPEG
- Aslan, N., Ceylan, B., Koç, M.M., Findik, F.: Metallic nanoparticles as X-ray computed tomography (CT) contrast agents: a review. J. Mol. Struct. 1219, 128599 (2020). https://doi.org/10.1016/J.MOLSTRUC.2020.128599
- Lusic, H., Grinstaff, M.W.: X-ray-computed tomography contrast agents. Chem. Rev. 113(3), 1641–1666 (2013). https://doi.org/ 10.1021/CR200358S/ASSET/IMAGES/MEDIUM/CR-2011-00358S\_0030.GIF
- 109. Xiao, Y.D., Paudel, R., Liu, J., Ma, C., Zhang, Z.S., Zhou, S.K.: MRI contrast agents: classification and application (review). Int. J. Mol. Med. (2016). https://doi.org/10.3892/ijmm.2016.2744
- Brenizer, J.S., Hosticka, B., Berger, H., Gillies, G.T.: The use of contrast agents to enhance crack detection via neutron radiography. NDT E Int. 32(1), 37–42 (1999). https://doi.org/10.1016/ S0963-8695(98)00024-3
- Pugliesi, R., Andrade, M.L.G.: Study of cracking in concrete by neutron radiography. Appl. Radiat. Isot. 48(3), 339–344 (1997). https://doi.org/10.1016/S0969-8043(96)00229-1

**Publisher's Note** Springer Nature remains neutral with regard to jurisdictional claims in published maps and institutional affiliations.

